Interference Analysis Between mmWave Radars and IEEE802.11AD at 60GHz Unlicensed Bands

by

Shiyu Cheng

A Thesis

Submitted to the Faculty

of the

WORCESTER POLYTECHNIC INSTITUTE

In partial fulfillment of the requirements for the

Degree of Master of Science

In

Electrical and Computer Engineering

by

_____

May 2022

COMMITTEE MEMBERS:

_____

Professor Kaveh Pahlavan, Major Thesis Advisor, ECE Department, WPI

_____

Professor Seyed (Reza) Zekavat, Committee Member, Physics Department, WPI

_____

Professor Ali Abedi, Committee Member, ECE Department, University of Maine

_____

Professor Andrew Clark, Committee Member, ECE Department, WPI

Abstract

The IEEE 802.11ad standard operates at the 60GHz band. The frequency band covers from 57.24 to 70.20 GHz, which is subdivided into 6 channels, and the bandwidth for each channel is 2.16 GHz. The Texas Instruments (TI) mmWave radar operates at 60-64 GHz spectrum. The mmWave radar is widely used for gesture and motion detection as well as in the automotive industry for short-range collision detection. IEEE 802.11ad supports up to 6.75 Gbps short-range communications. IEEE 802.11ad and the mmWave radar operate at overlapping unlicensed spectrums, and naturally, they interfere with each other. A systematic analysis of interference between a communication link and a radar is a complex problem because both devices benefit from multiple-input and multiple-output (MIMO) antenna systems with beamforming. This thesis presents an empirical analysis of the mutual interference between the IEEE 802.11ad communication link and the TI mmWave radar. The thesis presents the impact of the IEEE 802.11ad communication link on the mmWave radar coverage and precision. It studies and models mmWave radar interference on the IEEE 802.11ad wireless communication packet loss rate. The thesis develops and models interference based on the angle between the interfering antennas. It analyzes the effects of IEEE 802.11ad on the coverage and precision of the radar measured by the Cramer-Rao Lower Bound. The thesis uses a testbed for empirical measurement of the packet loss rate of the IEEE 802.11ad as a result of its interference with a mmWave radar.

Acknowledgements

In this thesis, I describe the research I conducted in pursuit of my Master of Science Degree in Electrical and Computer Engineering in Worcester Polytechnic Institute.

Firstly, I would like to express my sincere gratitude to my research advisor, Professor Kaveh Pahlavan, for leading me into the research world. He always kindly offers his help and shares his experience with me. It is my greatest honor to have him as my advisor.

I am really grateful that I can have Professor Seyed A. Zekavat, Professor Ali Abedi, and Professor Andrew Clark as my committee members. Thank you for the valuable comments and reviewing of this thesis.

I also want to thank all the peers in lab CWINS, Zhuoran Su and Haowen Wei. Thank them so much that they offer me such a nice atmosphere in the lab like a family.

At last, I would like to dedicate my thesis to my beloved parents, who offer me totally understanding, support, and infinite love.

Contents

List of Figures

List of Tables

Chapter 1

1. Introduction

Since the Third Industrial Revolution, which occurred in the late 20th century, more advanced digital techniques have been developed to improve people's lives. Among these amazing techniques, wireless communication and localization play a fundamental role, which is the reason why we call this the "information age." Millions of innovative applications are developed based on wireless communication systems and localization information, which have been bringing incredible and fundamental impact on people's lives these years. For the wireless communication systems, at the time of this writing, we have two different classes to connect devices to the Internet, which are the IEEE 802.11 wireless local area networks, commercially known as Wi-Fi, and cellular mobile data networks. In most scenarios, especially those indoor environments, Wi-Fi is a better choice because it can provide a higher data rate, a more reliable connection, and a lower cost compared with cellular networks.

In [1] , the authors introduced a historical perspective on the evolution of Wi-Fi technology. The pioneering research about wireless data communications for office information networks emerged in the mid-1980s [2] [3] , and the IEEE 802.11 standardization activity for wireless local area networking began in the late 1980s [4] . After that, in the late 1990s, the IEEE 802.15 standardization activities introduced Bluetooth, Zigbee, and Ultra-Wideband (UWB) technologies for personal area networking [5] . With the development of wireless technology, the millimeter wave (mmWave) technology was introduced to support wireless communication at high data rates up to multiple gigabits per second. Nowadays, billions of smart devices such as smartphones, laptops, and iPad are connected to the Internet through Wi-Fi access points. Based on that, people can get information from the Internet, and more and more applications are developed to meet people's needs.

A wireless communication system transmits symbols, and each symbol carries a limited number of bits of information. These symbols, carrying packets of information, are sent from the transmitter to a receiver or multiple receivers. All the suitable devices located in the transmitter's coverage area can receive the packets sent from the transmitter. In the indoor scenarios, the received signal arrives through different paths, including not only the direct path but also the paths reflected by the ceiling, floor, and walls.

This research has been partially supported by the NSF SII-2037782.

Apart from communication systems, radar systems are also very important in the field of wireless technologies. Similar to communication devices, radars also transmit electronic waveforms. Nevertheless, the transmitter and receiver are deployed at the same location, as shown in Fig. 1.1. Radars compare the characteristics of the received signals with those of transmitted signals to get information about surrounding objects in the environment.

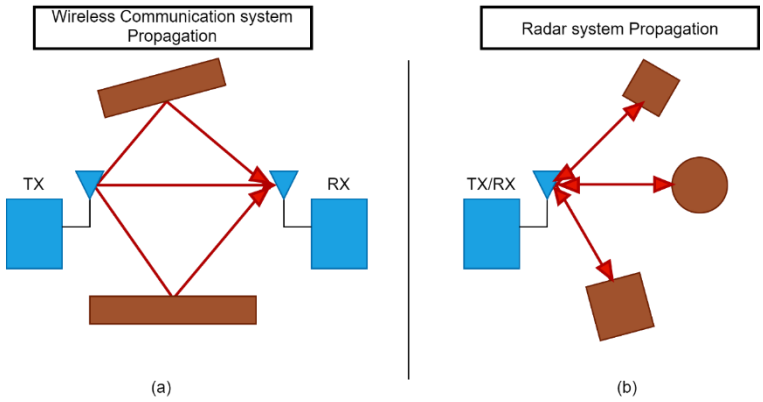

Figure 1. 1: Two classes of wireless devices: (a) Wireless communication system, with transmitter (Tx) and receiver (Rx) in different locations, and (b) Radars system with integrated Tx and Rx.

In both the communication and radar systems, receivers can measure the characteristics of the radio frequency (RF) propagation, such as magnitude, phase, and time of arrival of multipath. Firstly, all these measurements can be used to analyze the quality and coverage of wireless communication and the accuracy and coverage of radar systems. Besides, these measurements can also be used to develop many innovative applications which are of great benefit to people's life.

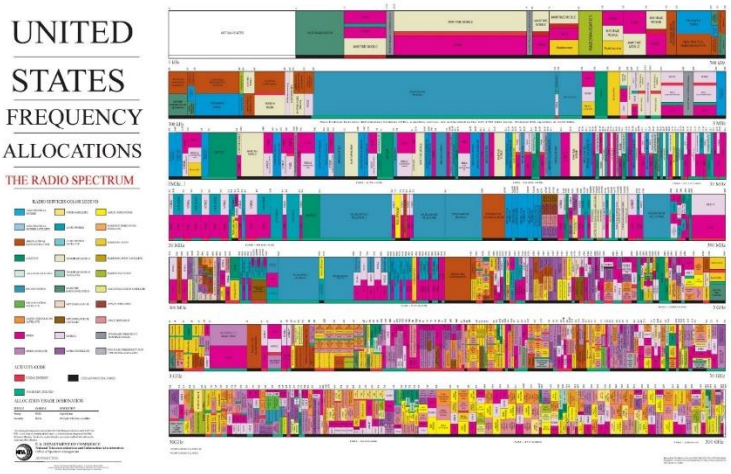

Figure 1. 2: United States Frequency Allocations Chart 2016

However, as shown in Fig. 1.2, many unlicensed bands are used for multiple systems because of the restriction of the spectrum resource [6] . Therefore, analysis of the interference between different systems which are working on the same bands is very important. Intelligence spectrum management and regulations have recently attracted considerable attention [7] . A new paradigm is evolving for this purpose, and the core for the evolution of this is understanding the real meaning of interference among RF devices contributing to the spectrum. These RF devices are divided into wireless communications (Wi-Fi, cellular wireless) and wireless positioning systems (radars and GPS). Cellular wireless and GPS operate in licensed bands, while Wi-Fi and short-range radars operate in unlicensed bands. Interference is inherent to unlicensed band operation when devices are in proximity to each other. Analysis of this interference is complex because it involves physical and medium access control of Wi-Fi as well as details of signal design for the radars. IEEE 802.11ad standard uses mmWave frequency to support high data rate, which can be used to apply in innovative applications, and mmWave radars are also widely used in industrial fields. For example, Texas Instruments (TI) has developed a short-range mmWave radar based on this technology [8] . People use it to get the location, speed, or other information of the objects, which can be used to produce many applications in the fields such as the autonomous cars system, gesture, and motion detection technologies. Therefore, it is important to analyze the interference between these two systems, which are working on the same frequency band. In [9] , authors analyze the interference between IEEE802.11ad and mmWave radar in a lab scenario. In this thesis, we provide a methodology for analyzing the interference between IEEE

802.11ad and TI mmWave Radar operation around 60GHz in lab and corridor scenarios.

1.1 Motivation

The IEEE 802.11ad standard operating at 60 GHz unlicensed band supports multi-gigabit-per-second throughput [10] . It uses beamforming to deal with the problem of high attenuation. Benefitting from the multi-gigabit-per-second throughput of the IEEE 802.11ad, many novel applications are developed. With the appearance of IEEE 802.11ad devices, people can download large documents from the cloud at high speed, enjoy video games using virtual reality (VR) devices with higher performance, and exchange large files with each other at higher data rates. Besides, the growth of the wireless networking industry paved the way to the commercial success of low-cost mmWave radars operating on unlicensed bands. They have been leveraged in modern cyberspace applications such as human-computer interaction [4] , gesture and motion detection, authentication, and security. Short-range mmWave radar operating at 60-64 GHz is a crucial technology on the Internet of things (IoT) for its capability of detecting the range, velocity, and angle of objects with sub-millimeter range accuracy. Since the unlicensed 60 GHz band is used for both IEEE 802.11ad and mmWave radar, the interference generated by the coexistence of various technologies should be analyzed. There are four types of interference on the 60 GHz band: IEEE 802.11ad to IEEE 802.11ad, mmWave radar to mmWave radar, IEEE 802.11ad to mmWave radar, and mmWave radar to IEEE 802.11ad. In [11] , authors analyze the interference between multiple IEEE 802.11ad devices. In that thesis, the interference caused by multiple 60 GHz infrastructure to vehicle communication links is analyzed, and the impact of the communication quality, such as the real-time transmission of high-definition video streams, is estimated.

However, few studies have analyzed the interference between the IEEE 802.11ad and mmWave radar. Due to the reciprocity of the channel, both IEEE 802.11ad and chirp radar devices interfere. This interference may lead to packet loss in communication systems and a significant drop in the maximum detection range in mmWave radars.

1.2 Contribution

In this thesis, we present a methodology for analytical and empirical analysis of mutual interference between IEEE 802.11ad wireless communication devices and the mmWave radars operating on 60GHz unlicensed bands. We examine IEEE

802.11ad and TI mmWave radar interference via designing a testbed. The rest of this paper is organized as follows. The report consists of two major sections and the major contribution of this report has been listed as follows:

- Design a testbed to measure and model the interference between IEEE802.11ad and TI mmWave radar systems
- Analysis the IEEE 802.11ad interference on mmWave radar.
- Analysis the mmWave radar interference on IEEE 802.11ad

1.3 Thesis Outline

The following chapters are organized as follows: In Chapter 2, we analyze how the IEEE 802.11ad communication link influences the coverage and precision of the TI mmWave radar. The model of interference is built based on the distance and the angle-of-arrival (AOA) of IEEE 802.11ad communication link. We analyze the influence on the coverage and precision of the radar based on the signal to the interference ratio (SIR) and Cramer-Rao Lower Bound (CRLB). When the interference source is close to the radar in lab scenario, the detection range of the radar will decrease, but the detection coverage of the mmWave radar will not decrease significantly in a corridor scenario. The distance measurement errors of those detected objects do not change. In Chapter 3, we analyze how the TI mmWave radar interferes with IEEE 802.11ad communication. An interference time ratio model is used to analyze the increase of the packet loss rate of the IEEE 802.11ad communication when interference from the mmWave radar is introduced. By tuning the frame rate of the radar, we change the time ratio of the interference. The empirical measurement of packet loss rate is compared with the analytical results based on the interference time ratio model. With the increase of the frame rate, the packet loss rate (PLR) increases as well. When the frame rate is 30 frames per second, the experimental PLR is 18%, and the analytical PLR is 15.55%. Finally, we conclude our work in Chapter 4.

Chapter 2

2. Background

Historically interference in the unlicensed band was first addressed by the IEEE 802.15.2 to analyze the interference between IEEE 802.11b and Bluetooth for wireless communications and some pioneering studies of this interference are available in [12] . In 2001, the authors found that it was unfeasible for the IEEE 802.11b DSSS and Bluetooth radios to reliably operate simultaneously in the same computer because these two systems will interfere with each other significantly. For both data and voice transmission, the packet error rate was 99% and the throughput was reduced virtually to zero once the radios were turned on. The Ping time did not even register. This indicates the complete elimination of reliability for the 802.11b DSSS as well as Bluetooth when operating on the same computer. And the authors state that to make two systems work at the same time, it is necessary to keep IEEE 802.11b DSSS and Bluetooth radios at least three meters apart.

Wi-Fi and Bluetooth are communications devices, analysis of interference between radar and a wireless communication system is different and more complex. An analysis of the interference from Worldwide Interoperability for Microwave Access (WiMAX) to next-generation weather radars operating on licensed bands is available in [13] . This report describes an investigation for radio frequency interference from communication systems to radars systems operating in another band and gives a solution for this problem. This report analyzes the interference from BRS/EBS base station, which is operating in the BRS/EBS Upper Band Segment (UBS) of 2614-2690 MHz and emitting orthogonal frequency division multiplexed (OFDM) WiMAX signals, to the NEXRAD radars.

In this report, it is shown that the out-of-band (OOB) emissions from BRS/EBS base station can cause interference to NEXRAD receivers. This report analyzes the power levels that will result in interference to the NEXRAD receivers. It also provides a method to measure the power of interference.

When analyzing the interference between communication and radar systems on a licensed band, people focus on the OOB interference because the frequency bands are well arranged. When analyzing the interference between communication and radar systems on unlicensed bands, the interference generated by the overlapped working frequency bands plays an important role. Some papers focus on this field which is introduced in the related works section.

2.1 Comparison of Wireless Network and Radar

A wireless network is a computer network that uses wireless data communications between network nodes. Compared with cables, using wireless network costs less when people use multiple devices which need to be connected to the Internet. Wireless networks mainly include cellular network, wireless personal area networks (WPANs), and wireless local area networks (WLANs). For the cellular network, it is a radio network distributed over land areas called cells. In each cell, at least one transmitter is located to transmit the data to users. Although cellular network was originally designed for cell phone, however, with the development of the smartphones, cellular networks also provide data service. In [1] [14] , the authors give us an introduction to the evaluation of the networks. The idea of a WLAN was first introduced in 1970s as a method for local area networking in manufacturing areas, and at that time Diffuse infrared (IR) technology was used [15] . After that, a prototype WLAN using direct sequence spread spectrum (DSSS) with surface acoustic wave (SAW) devices were introduced [16] . Later, the ALOHA system, which is considered as the first experimental wireless data network was introduced [17] . Besides, the development of WLAN prospers with the release of unlicensed ISM bands. With the appearance of IEEE 802.11 standards, the data rate increased from 2 Mb/s to 11 Mb/s with the release of IEEE 802.11b. And IEEE 802.11 a/g and n support 54 Mb/s and over 100 Mb/s respectively. Recently, with the development of mmWave technology, IEEE 802.11ad was introduced which can even support several gigabits per second.

Radar is a detection system that uses radio waves to determine the distance, angle, and velocity of objects. It can be used in many different fields such as aircraft, ships, spacecraft, motor vehicles, etc. A radar system includes a transmitter to produce electromagnetic waves and a receiver and processor to determine the information of the objects based on the reflected electromagnetic wave. The power received at the receiver of radar is P_r, which can be represented as:

$$P_r = \frac{P_t G_t A_r \sigma F^4}{(4\pi)^2 R_t^2 R_r^2}, \tag{1}$$

where P_t is the transmitter power, G_t is the gain of the transmitting antenna. A_r is effective aperture (area) of the receiving antenna., which can also be expressed as $\frac{G_r \lambda^2}{4\pi}$, where λ is transmitted wavelength, and G_r is gain of receiving antenna.

In (1), σ is radar cross section, or scattering coefficient of the target. F is pattern propagation factor. R_t and R_r are the distance from the transmitter to the target and the distance from the target to the receiver respectively. In (1), $F = 1$ is a simplification for transmission in a vacuum without interference. The value of propagation factor depends on the environment in which the system works.

2.2 Wi-Fi and mmWave radar

Wi-Fi is a family of wireless network protocols, based on the IEEE 802.11 family of standards. Wi-Fi is mainly used for WLAN devices that allow the nearby devices to exchange data by the Wi-Fi signal. This is widely used around the world that helps smartphones, laptops, desktops to connect the Internet. Recently, the Wi-Fi alliance consisted of more than 800 companies from the whole world.

Wi-Fi uses multiple parts of the IEEE 802 protocol family and is designed to interwork with Ethernet. Devices can connect to other devices through wireless access points. The different versions of Wi-Fi are specified by different IEEE 802.11 protocol standards. For different IEEE 802.11 protocol standards, the radio bands, the maximum ranges, and speeds may be different from each other. Nowadays, most Wi-Fi devices are working on the 2.4 gigahertz and 5 gigahertz frequency bands; these bands are subdivided into multiple channels. Different networks can share the same channel, however, only one transmitter transmits on a channel at the same time locally.

The millimeter wave (mmWave) radar is a special class of radar that works on high-frequency bands using very short wavelength electromagnetic waves. Radar systems transmit electromagnetic wave signals and then receive the signal reflected from objects. By capturing the reflected signal, a radar system can determine the distance between the radar and objects, as well as the velocity and angle of the objects.

There are some specific advantages of mmWave radar systems. Firstly, the wavelength sent by the mmWave radar is in the millimeter range, which is very short. This feature makes the size of system components such as the antennas required to process mmWave signals small. Another advantage of short wavelengths is the high accuracy. A mmWave system will have the ability to detect movements that are as small as a fraction of a millimeter.

2.3 Related works

Some works focus on the analysis of the interference between communication and frequency-modulated continuous-wave (FMCW) radar, which works on unlicensed bands. In [18] , authors present a study about the FMCW radar interference on the IEEE 802.11n Wi-Fi communication. They set the FMCW radar as the interference source and change the interference to signal power ratio (ISR). Researchers use this method to analyze the radar signals that interfere with the orthogonal frequency-division multiplexing (OFDM) signals and understand how specific parameters of the interference signal can interfere on the communication. The authors analyze the relationship between the setting of the interference through the signal processing at the reception. In that paper, researchers introduced a method for agile communication solutions through reconfiguring the signal processing to reduce the impact of interference signals. In that scenario, an IEEE 802.11n wireless network gets interference from an FMCW signal. The FMCW interference signal sweeps across the given frequency band. Authors analyzed the interference to signal power ratios when the different sweep periods are applied. A set of measurements was performed to evaluate the performance of the communication network under different interferences. Authors measure bit rate to test the interference characteristics on communication quality. With the increase of the ISR, the bit rate for the IEEE 802.11n decreases.

In [19] , authors analyze the interference between automotive radar and vehicular communication. In this scenario, both radars and wireless communication are susceptible to interference. The authors first analyze the mutual interference of spectrally coexistent frequency modulated continuous wave (FMCW) radar and communication systems theoretically. The model of occurrence probability is used to explain the impact of interference. And then authors introduce a method to combine the radar and communication systems to mitigate the interference, which is named as RadChat. RadChat is a distributed networking protocol to cooperate radar and communication systems to mitigate interference among FMCW-based automotive radars, including self-interference. The results show that RadChat can significantly reduce mutual interference in single-hop vehicular networks.

When considering the communication interference on the radar, authors analyze the relationship between the signal-to-interference-plus-noise ratio (SINR), the probability of detection, and the probability of false alarm (ghost targets). When considering the radar interference on the communication, authors analyze the relationship between the SINR and the symbol error probability. All these works

motivate researchers to analyze the interference between radar and communication links working on the same band.

Authors in [20] assess two types of interference between multiple mmWave radar devices which are the crossing interference and the parallel interference. This paper discusses the problem of radar-to-radar interference and how it can be managed in TI radar devices. Interference is a major issue for reliable radar functioning, as the number of deployed radars has increased in both automotive and industrial contexts. Thus, the likelihood that one radar's transmission is received by another radar has also increased. Interference results in a host of issues, such as a degradation in the noise floor leading to missed detections, or blind spots at certain ranges or directions. It can also create ghost objects in certain cases (ghost targets are targets seen by the radar which do not exist). The crossing interference will be introduced when the victim radar and the aggressor radar have different slopes that the chirps of them cross each other. In this situation, the noise floor of the radar will increase, therefore, it will reduce the signal-to-noise ratio (SNR) of strong targets and bury weak targets. Besides, the parallel interference will be introduced when the victim radar and the aggressor radar have the same slope and the starting time of them is very close. In this situation, a ghost target will be detected in the system, which does not really exist.

2.4 IEEE 802.11ad and TI mmWave radar

As the spectrum source becomes restricted, some unlicensed bands allow for dual-purpose use, such as the 60 GHz unlicensed band. The 60 GHz unlicensed band is used for IEEE 802.11ad WiGig communication under restrictions in terms of power emissions, and it is also used for radar [21] [22] . The coverage of radar and wireless communication systems in mmWave bands can provide benefits for both applications. However, a dual-use system must account for four types of interference: radar-to-radar (R2R), communication-to-communication (C2C), communication-to-radar (C2R), and radar-to-communication (R2C). In this thesis, we mainly analyze the C2R interference and R2C interference.

2.4.1 IEEE 802.11ad

IEEE 802.11ad is characterized by highly directional transmission enabled by beamforming [23] . According to the Friis transmission equation, 60 GHz propagation has a significant high path loss because of its high signal frequency. In

contrast, oxygen absorption plays a minor role over short-range distances, even though it works on the 60GHz band [24] . Besides, in IEEE 802.11ad communication, received signals are dominated by the line of sight (LOS) path and first-order reflections from strong reflecting materials. As an example, metallic surfaces were found to be strong reflectors and allow non-LOS (NLOS) communication [25] . However, other materials, such as concrete materials, cause significant signal attenuation and can easily create a blockage. Thus, 60 GHz communication is more suitable to indoor environments.

The IEEE 802.11ad has some important features. Firstly, it defines a directional communication scheme that takes advantage of beamforming to resolve the problem of high path loss. This standard introduces a novel concept of "virtual" antenna sectors [26] that discretize the antenna azimuth. A sector focuses antenna gain in a certain direction.

For the IEEE 802.11ad PHY layer, three different PHY layers are applied in different scenarios. The control PHY is designed for a low signal-to-noise ratio (SNR) before beamforming. The single carrier (SC) PHY is used in the scenario with a power-efficient and low-complexity transceiver. The low-power SC PHY replaces the low-density parity check (LDPC) encoder by a Reed-Solomonencoder for further reducing process power. The orthogonal frequency-division multiplexing (OFDM) PHY provides high performance in frequency selective channels, it can achieve the maximum 802.11ad data rates. For different MCS, the data rates are shown in Table 2.1, Table 2.2, and Table 2.3. Despite having different PHYs, all of these PHY layers share the same packet. The bandwidth for IEEE 802.11ad is 2.16 GHz which is 50 times wider than the channels available in 802.11n. And the packet structure for IEEE 802.11ad is shown in Fig. 2.1. The packet includes some typical structures as other IEEE 802.11 schemes, for example, it has a short training field (STF) and a channel estimation field (CEF), which are followed by the PHY header, PHY payload, and a cyclic redundancy check (CRC). Finally, optional automatic gain control (AGC) and training (TRN) fields might be appended. These two parts are unique to IEEE 802.11ad which are used for beamforming. For the STF, the control PHY has 48 Golay sequences, each 128 samples long. And the SC and OFDM PHY have 17 Golay sequences. The CEF has 9 Golay sequences and a different combination of Golay sequences is used by OFDM PHY to distinguish it from SC PHY.

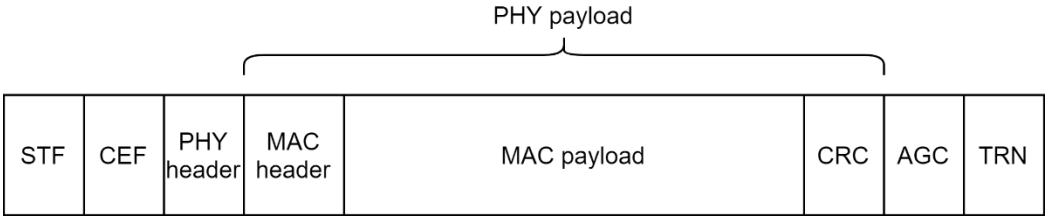

Figure 2. 1: IEEE 802.11ad packet structure

Table 2. 1: Modulation and coding scheme for the control PHY

MCS index	Modulation	Code rate	Data rate
0	DBPSK	$1/2^a$	27.5 $Mbps^a$

Table 2. 2: Modulation and coding scheme for the OFDM

MCS index	Modulation	Code rate	Data rate (Mbps)
13	SQPSK	1/2	693.00
14	SQPSK	5/8	866.25
15	QPSK	1/2	1386.00
16	QPSK	5/8	1732.50
17	QPSK	3/4	2079.00
18	16-QAM	1/2	2772.00
19	16-QAM	5/8	3465.00
20	16-QAM	3/4	4158.00
21	16-QAM	13/16	4504.50
22	64-QAM	5/8	5197.50
23	64-QAM	3/4	6237.00
24	64-QAM	13/16	6756.75

Table 2. 3: Modulation and coding scheme for the SC

MCS index	Modulation	Code rate	Data rate (Mbps)
1	BPSK	1/2	385
2	BPSK	1/2	770
3	BPSK	5/8	962.5
4	BPSK	3/4	1155

5	BPSK	13/16	1251.25
6	QPSK	1/2	1540
7	QPSK	5/8	1925
8	QPSK	3/4	2310
9	QPSK	13/16	2502.5
10	16-QAM	1/2	3080
11	16-QAM	5/8	3850
12	16-QAM	3/4	4620

The control PHY defines modulation and coding scheme (MCS) 0. The throughput of it is 27.5 Mb/s. The $\pi/2$-differential binary phase shift keying (BPSK) modulation is used in control PHY. All devices, which support IEEE802.11ad, can use mandatory control PHY to communicate before establishing a high data rate communication link. The control PHY is used to transmit and receive frames such as beacons, information request and response, probe request and response, sector sweep, sector sweep feedback, and other management and control frames.

The devices with low complexity and energy-efficient can use SC PHY (MCS 1-12) and low-power SC PHY (MCS 25-31) to transmit data, and the throughput of them is up to 4.62 Gb/s. The devices with complex and energy-intensive structures can use the optional mode, OFDM PHY (MCS 13-24), to achieve a maximum throughput up to 6.75 Gb/s. This PHY uses 64-QAM and a rate 13/16 code to achieve the highest 802.11ad data rate.

Besides, for each scheme, the received power should fit the receiver sensitivity which is shown in Table 2.4.

Table 2. 4: Receiver sensitivity for different MCS

MCS index	Receive sensitivity (dBm)
0	-78
1	-68
2	-66
3	-65
4	-64
5	-62
6	-63
7	-62
8	-61
9	-59
10	-55
11	-54
12	-53
13	-66
14	-64
15	-63
16	-62
17	-60
18	-58
19	-56
20	-54
21	-53
22	-51
23	-49
24	-47
25	-64
26	-60
27	-57
28	-57
29	-57
30	-57
31	-57

2.4.2 TI mmWave radar

Historically, radar used discrete components, such as power amplifiers, low-noise amplifiers, etc. However, nowadays, more integrated solutions are becoming available. These radars integrate all radio frequency (RF), analog functionality, and signal processing (DSP) capability into a single chip, making this on-chip solution perform well in the market. Because of its high integration, this solution significantly simplifies the radar sensor implementations, which makes it has a compact form and cost-effective. TI offers a series of highly integrated radars working on mmWave bands. These devices are widely used in automotive and industrial radar markets [27] .

Frequency Modulated Continuous Wave (FMCW) mmWave radar sensors are becoming increasingly popular these days. These radars are used in multiple automotive and industrial applications. Different data provided by the FMCW radars could be used in these applications, such as target distance, range resolution, Doppler-Range Heat map, etc. Understanding the mechanisms of the FMCW chirp configuration and system performance parameters helps users set the proper chirp configurations and collect the data they need to develop applications.

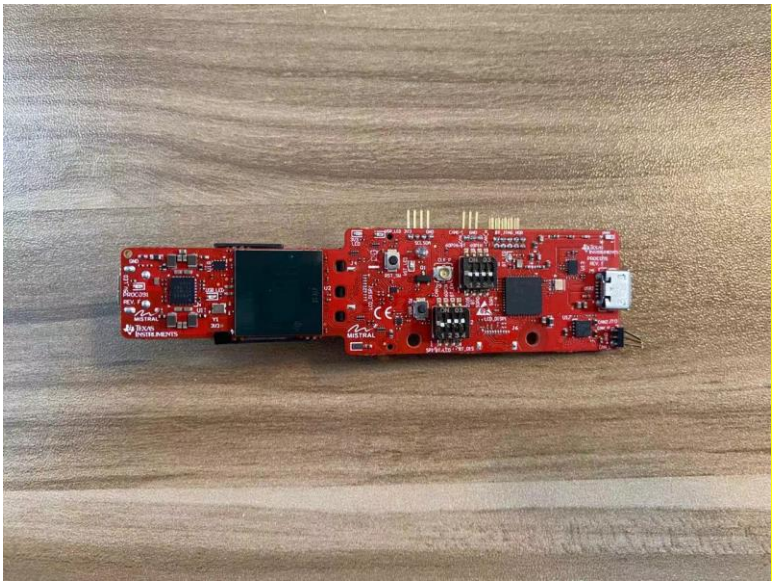

Figure 2. 2: IWR6843aopevm: The IWR6843 antenna-on-package (AoP) evaluation module (EVM)

TI’s mmWave radar devices provide large flexibility in setting different chirp configurations. The digital timing engine and a built-in radio processor are used to

control the timing parameters with high accuracy. In this thesis, we use IWR6843aopevm to set up the testbed, which is shown in Fig. 2.2.

In linear FMCW radars, the frequency of the transmitter (TX) signal changes linearly with time. The signal sweeps the bandwidth, which is referred to as a chirp. Between every two chirps, there is an inter-chirp idle time. Each frame contains a series of chirps followed by inter-frame idle time. Frame rate represents the number of frames in one second. The various parameters of the chirp ramp, such as frequency slope and sweep bandwidth, can be set as different values based on the needs of different applications.

2.5 Measurement tools

In this section, two measurement tools are used to get the information needed in this experiment. The mmWave Demo Visualizer is an application that can show the power of the signal and noise and the distances between objects and radar [28] . The Iperf3 is a tool to measure the data rate under TCP and packet loss rate under UDP.

2.5.1 mmWave Demo Visualizer

The mmWave Demo Visualizer, which is shown in Fig. 2.3, is provided by TI and it is developed for the mmWave radar to show the information of detected objects. There are several sliders in this application that can be set as different values, which are frame rate, range resolution, maximum unambiguous range, maximum radial velocity, and radial velocity resolution. In this thesis, we use the best range resolution scene.

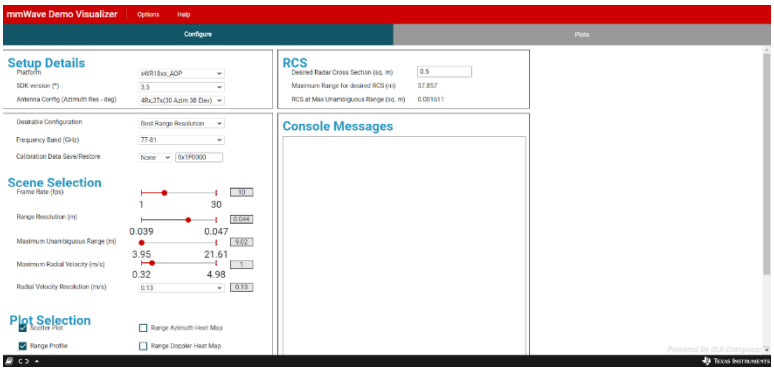

Figure 2. 3: TI mmWave Demo Visualizer Panel

Frame rate slider is used to select the rate at which the measurement data must be shipped out of the mmWave device. Range resolution slider is used for the user to

select the desired range resolution in meters. It is the minimum distance to distinct two objects. For the maximum unambiguous range, it is a slider for users to select the farthest distance you expect to detect objects. Maximum Radial Velocity is a slider to represent the maximum radial velocity users expect targets to be moving in within the radar field of view.

2.5.2 iperf3

Iperf is a network testing tool used to create Transmission Control Protocol (TCP) and User Datagram Protocol (UDP) data streams. It can be used to measure the throughput of a network under TCP and measure the packet loss rate of a network under UDP. To measure the bandwidth utilization at the transport layer, the iperf uses a client-server architecture where the Iperf client connects to Iperf server [29] [30] .

In this thesis, to test the packet loss rate, the Iperf3 is run in such way that the data are continuously sent from the transmitter to the receiver. The experiments begin with the Iperf client continuously sending a UDP stream to the Iperf server over the IEEE 802.11ad network.

2.6 Cramér–Rao Lower Bound

In estimation theory and statistics, the Cramer-Rao Lower Bound (CRLB) expresses a lower bound on the variance of unbiased estimators of a deterministic parameter. In this thesis, we use CRLB to determine the accuracy of the radar system.

The CRLB calculates the bound on the estimation of the variance of the distance measurement error (DME) [31] . The maximum likelihood (ML) estimate provides the best estimate, and the CRLB provides an analytical tool for calculation of the bounds on the variance of the ML estimate. Therefore, if we use any other algorithm to estimate the distance, the CRLB provides a universal lower bound to our estimation and we can use it as a benchmark for evaluation of the performance of any estimation algorithm that we may use, either for simplicity or practicality.

The CRLB allows for comparing the precision of location estimations by alternative approaches for localization. The smaller the variance, the smaller the chance that the error in location estimate is large. The basic formulation of single parameter estimation using observation of a function of a parameter in zero-mean additive Gaussian noise in classical estimation theory. The analysis begins with a desire to estimate the parameter, α, when we observed, O, its function, $g(\alpha)$, in zero-mean Gaussian noise, η with a standard deviation of σ.

$$O = g(\alpha) + \eta(\sigma). \tag{2}$$

In classical estimation theory, there are two popular methods to calculate the estimate of the parameter $\hat{\alpha}$: Maximum Likelihood (ML) estimation and the Minimum Mean Square Error (MMSE) estimation. In ML estimation, the likelihood function is:

$$f(O/\alpha) = \frac{1}{\sqrt{2\pi}\sigma} e^{-\frac{[O-g(\alpha)]^2}{2\sigma^2}}. \tag{3}$$

The CRLB can be calculated by inverting the Fisher Information Matrix (FIM):

$$CRLB = \text{var}[\hat{\alpha}(O) - \alpha] \geq F^{-1}. \tag{4}$$

The FIM matrix, which is actually scalar in single parameter estimation, is given by

$$F = E[\frac{\partial \Lambda(O/\alpha)}{\partial \alpha}]^2 = -E[\frac{\partial^2 \Lambda(O/\alpha)}{\partial \alpha^2}], \tag{5}$$

in which $\partial\Lambda(O/\alpha)$ is the log likelihood function in ML estimation process.

To calculate the CRLB for range estimation using the measurement of the RSS, we need to calculate the log likelihood function of observation of the function of a parameter in noise given by equation. For the observation of the function of a parameter, $g(\alpha)$, in zero mean Gaussian noise with standard deviation of, σ, the FIM and the CRLB are given by:

$$\begin{cases} F = -E[\frac{\partial^2 \ln f(O/\alpha)}{\partial x^2}] = E[\frac{\partial \ln f(O/\alpha)}{\partial x}]^2 = \frac{[g'(\alpha)]^2}{\sigma^2} \\ CRLB \geq F^{-1} = \frac{\sigma^2}{[g'(\alpha)]^2} \end{cases} \tag{6}$$

Chapter 3

3. Methodology

In this chapter, the interference between IEEE 802.11ad and mmWave radar is analyzed. The background of these two technologies is introduced. In section 3.1, the theoretical models of the power of the signal and the power of interference are analyzed, and based on that, the influence of coverage and the accuracy of the radar system is analyzed based on the SNR and CRLB. After that, the testbed to validate IEEE 802.11ad interference on the mmWave radar system is designed.

In section 3.2, the interference time ratio is introduced to analyze how the mmWave radar influences IEEE 802.11ad performance. Iperf3 is used to test the change of packet loss rates which reflects the increase in the packet loss rate of IEEE 802.11ad system when the mmWave radar is introduced.

3.1 IEEE 802.11ad interference to mmWave radar

In this section, the frame structure of the mmWave radar is introduced. To analyze the interference on the mmWave radar system, we focus on two aspects, the interference on the coverage and the interference on the accuracy. The change of the mmWave radar coverage is changed based on the change of the SINR. Besides, we use CRLB to analyze the interference on the accuracy of the mmWave radar system.

3.1.1 Introduction

The objective of this study is to measure the interference between the IEEE 802.11ad and mmWave radars operating in overlapping frequencies on unlicensed mmWave around 60 GHz bands. The IEEE 802.11ad standard supports wireless communications at unlicensed mmWave band which covers from 57.24 to 70.20 GHz. The frequency band has 6 subdivided channels, and the bandwidth for each channel is $B_c = 2.16GHz$, which supports the data rate up to 6.75 Gbps. The standard recommends MIMO antenna systems with beamforming capabilities to deal with high attenuations at 60 GHz. To conduct our experiments, we use a pair of IEEE 802.11ad RBwAPG-60ad devices at center frequency of 62.64 GHz, which are manufactured by Mikrotik. The short-range TI millimeter wave (mmWave) radar operating at 60-64 GHz [8] , whose bandwidth is $B_r = 4GHz$, has also emerged for short range micro-gesture and motion detection [4] as well as short distance ranging [32] . The mmWave radar uses short-wavelength electromagnetic waves to detect

objects based on the transmitted signals and the received signals, which are reflected from objects. These two devices interfere with each other, when their bands overlap.

To design our testbed, we used the TI's FMCW mmWave radar, which detects the position of the objects based on the frequencies of the transmitted signal and the received signal. Fig. 1 shows the structure of FMCW frames. In linear FMCW radars, the frequency of transmitter (TX) signal changes linearly with time. As shown in Fig. 3.1 and Fig. 3.2, the signal sweeps the bandwidth which is referred to as a chirp.

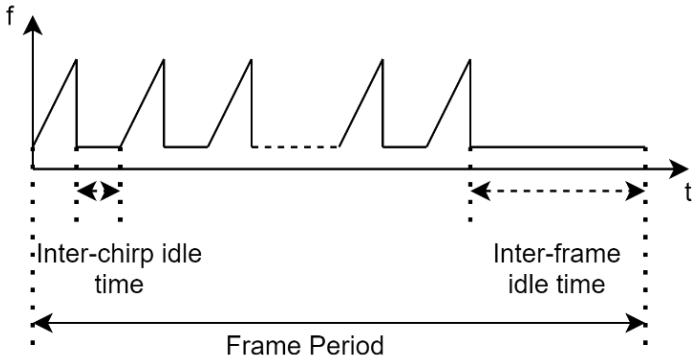

Figure 3. 1: Frequency-modulated continuous wave (FMCW) chirp radar frame structure for periodic sweep with inter-frame idle times as well as inter-chirp idle times

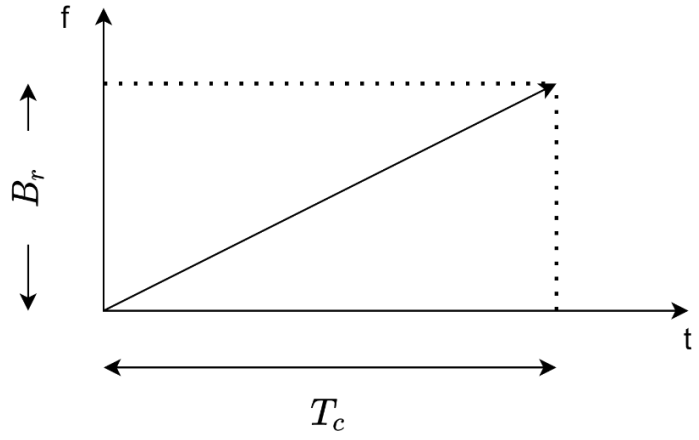

Figure 3. 2: The structure of a chirp

Between each two chirps, there is an inter-chirp idle time. In each frame, it contains a series of chirps and followed by inter-frame idle time. Frame rate represents the number of frames in one second. As shown in Fig. 3.3, an FMCW radar transmits a series of chirps and receives signals reflected from an object at the receiver (RX).

The RX signal is time delayed but has the same linear ramp form as the TX signal. The transmit signal is $x_{TX}(t)$ and the receive signal is $x_{RX}(t)$.

$$x_{TX}(t) = \cos(\omega_1 t + \phi_1), \tag{7}$$

$$x_{RX}(t) = \cos(\omega_2 t + \phi_2). \tag{8}$$

The FMCW radar mixes the TX signal and RX signal to generate the intermediate frequency (IF) signal, whose frequency is the difference between the instantaneous frequencies of the TX signal and RX signal.

$$x_{IF}(t) = A \times \cos[(\omega_1 - \omega_2)t + (\phi_1 - \phi_2)], \tag{9}$$

where A is the amplitude of the IF signal and the frequency of it is $(\omega_1 - \omega_2)$, and the phase is $(\phi_1 - \phi_2)$.

Therefore, the relationship between the frequency of the IF signal and the distance between the radar and the object is:

$$S \times \tau = \frac{2d \times S}{c} \tag{10}$$

, where S is the slope of the chirp, τ is the propagation delay, d is the distance between the radar and the object, c is speed of light. The range resolution represents the smallest distance between two objects that allows them to be detected as separate objects. The range resolution (R_{res}) of FMCW radar corresponds to:

$$R_{res} = \frac{c}{2B_r} \tag{11}$$

, where c is speed of light, and B_r is the sweep bandwidth of the chirp of the FMCW radar [8] .

The mmWave radar used in this paper is IWR6843AOPEVM, which works on the band from 60 GHz to 64 GHz. It can be used by vehicles to enjoy a safer driving experience and be used by specific applications to detect human gestures. With the development of the IoT industry, IEEE 802.11ad devices and mmWave radar will be widely used in our daily life.

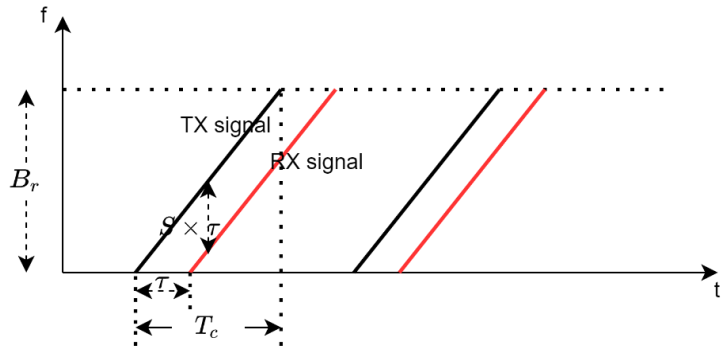

Figure 3. 3: The time-frequency relation between the transmitted and the received signal and their associated parameters, *S* is the slope of the chirp and τ is the propagation delay. The difference in transmitted and the received frequencies is $S \times \tau$, used to calculate the distance between objects and the radar.

3.1.2 Power of Signal and Interference Modeling

In this section, the theoretical received signal strength (RSS) is calculated based on the classical path loss function [33] :

$$\begin{cases} P_r = \dfrac{P_0}{d^{\alpha}} \\ P_r(dB) = P_0(dB) - 10\alpha \log_{10}(d) \end{cases}, \tag{12}$$

where *d* is the distance between the receiver and the transmitter, P_r and P_0 represent received signal strength at the distance of *d* and 1 meter respectively, and α is the gradient indicating the relation between distance and power. However, the RSS for the same distance from the transmitter will be different depending on the environment. The mean value of the RSS can be expected according to (3), however, the real value of RSS is around this value because of shadow fading. Therefore, when we take shadow fading into account, we can get (4):

$$P_r = P_0 - 10\alpha \log 10(d) + X(\sigma), \tag{13}$$

where $X(\sigma)$ is a Gaussian random variable with variance σ. In practice, we can use the Least Square (LS) method to get the path loss model parameters, (P_0, α, σ), based on the measured RSS.

In radars, we have two issues which are range and precision. The range is calculated from the signal to the interference plus noise ratio (SINR) and precision is affected by bandwidth, SINR, and measurement time. To analyze the SINR, the power of the

radar signal (P_S) and the power of the interference signal (P_I) should be calculated. The signal power is:

$$\begin{cases} P_S = \dfrac{P_{t_r} G_{TX_r} \sigma G_{RX_r} \lambda_r^2}{(4\pi)^3 d^4} \\ P_S(dB) = -40\log_{10}(d) + 10\log_{10} \dfrac{P_{t_r} G_{TX_r} \sigma G_{RX_r} \lambda_r^2}{(4\pi)^3} \end{cases}, \tag{14}$$

where P_{t_r} is the output power of the radar, G_{TX_r} and G_{RX_r} represent the antenna gains of the TX and RX of the radar, σ is the radar cross-section (RCS) of the object, λ_r is the wavelength of the radar signal, and *d* is the distance between the object and the radar.

And the power of the interference source is:

$$\begin{cases} P_I = \dfrac{P_{t_c} G_{TX_c} G_{RX_r} \lambda_c^2}{4\pi r^2} \\ P_I(dB) = -20\log_{10} r + 10\log_{10} \dfrac{P_{t_c} G_{TX_c} G_{RX_r} \lambda_c^2}{4\pi} \end{cases}, \tag{15}$$

where P_{t_c} and G_{TX_C} are the output power and antenna gain of the transmitter of the IEEE 802.11ad device, λ_c is the wavelength of the IEEE 802.11ad communication signal, and *r* is the distance between the radar and the IEEE 802.11ad transmitter. The value of G_{RX_r} is related to AOA.

Therefore, the SINR is:

$$\begin{cases} SINR = \dfrac{P_S}{P_I + P_N} \approx \dfrac{P_S}{P_I} \\ SINR(dB) \approx P_S(dB) - P_I(dB) \end{cases} \tag{16}$$

, where P_N is the power of thermal noise. As in this scenario, the mmWave radar is close to the IEEE 802.11ad TX, P_I is much stronger than P_N, the thermal noise is neglected.

3.3.3 CRLB Calculation

The IF signal will gets sampled by the analog to digital converter (ADC), suppose the sampling frequency is f_s. Before going through the ADC, the IF signal is

$$x_{IF}(t) = A \times \cos(2\pi f_b t + \phi), \tag{17}$$

where f_b is $\frac{1}{2\pi}(\omega_1 - \omega_2)$, ϕ is $(\phi_1 - \phi_2)$. After it gets through the ADC, the IF signal is:

$$x_{IF}[n] = A \times \cos(2\pi f_b n \frac{1}{f_s} + \phi), n = 0,1,2,...,N-1, \tag{18}$$

where N is the number of samples.

According to [34] , to calculate the CRLB for the range detection, the Fisher Information Matric for the discrete signal is:

$$[I(\theta)]_{ij} = \frac{1}{\sigma^2} \sum_{n=0}^{N-1} \frac{\partial x_{IF}[n;\theta]}{\partial \theta_i} \frac{\partial x_{IF}[n;\theta]}{\partial \theta_j}, \tag{19}$$

where $\theta = [A \; f_0 \; \phi]^T$, f_0 is $\frac{f_b}{f_s}$.

Therefore, we can calculate every component in this matrix as:

$$\begin{aligned} [I(\theta)]_{11} &= \frac{1}{\sigma^2} \sum_{n=0}^{N-1} \cos^2(2\pi f_0 n + \phi) = \frac{1}{\sigma^2} \sum_{n=0}^{N-1} \cos^2(\alpha) \\ &= \frac{1}{\sigma^2} \sum_{n=0}^{N-1} (\frac{1}{2} + \frac{\cos 2\alpha}{2}) \approx \frac{N}{2\sigma^2}, \end{aligned} \tag{20}$$

where α is $(2\pi f_0 n + \phi)$. An as the reason that:

$$\frac{1}{N^{i+1}} \sum_{n=0}^{N-1} n^i \sin(4\pi f_0 n + 2\phi) \approx 0, \tag{21}$$

$$\frac{1}{N^{i+1}} \sum_{n=0}^{N-1} n^i \cos(4\pi f_0 n + 2\phi) \approx 0. \tag{22}$$

Therefore, the components in this matrix can be calculated as:

$$[I(\theta)]_{12} = \frac{1}{\sigma^2}\sum_{n=0}^{N-1} -\cos(\alpha)\times A\times 2\pi n\times \sin(\alpha) = \frac{-A\pi}{\sigma^2}\sum_{n=0}^{N-1} n\sin 2\alpha \approx 0, \tag{23}$$

$$[I(\theta)]_{13} = -\frac{1}{\sigma^2}\sum_{n=0}^{N-1} A\times \sin(\alpha)\cos(\alpha) = -\frac{A}{2\sigma^2}\sum_{n=0}^{N-1}\sin(2\alpha) = 0, \tag{24}$$

$$[I(\theta)]_{21} = [I(\theta)]_{12} \approx 0, \tag{25}$$

$$[I(\theta)]_{22} = \frac{1}{\sigma^2}\sum_{n=0}^{N-1}(A\times 2\pi n)^2\sin^2(\alpha) = \frac{(2\pi A)^2}{\sigma^2}\sum_{n=0}^{N-1} n^2(\frac{1}{2}-\frac{\cos 2\alpha}{2}) \approx \frac{(2\pi A)^2}{2\sigma^2}\sum_{n=0}^{N-1} n^2. \tag{26}$$

Besides, as the reason that:

$$\sum_{n=0}^{N-1} n = \frac{N(N-1)}{2}, \tag{27}$$

$$\sum_{n=0}^{N-1} n^2 = \frac{N(N-1)(2N-1)}{6}. \tag{28}$$

The other components in this matrix can be calculated as:

$$[I(\theta)]_{23} = \frac{1}{\sigma^2}\sum_{n=0}^{N-1} 2\pi n\times A\times \sin(\alpha)\times A\times \sin(\alpha) = \frac{2\pi A^2}{\sigma^2}\sum_{n=0}^{N-1} n(\frac{1}{2}-\frac{\cos 2\alpha}{2}) \approx \frac{\pi A^2}{\sigma^2}\frac{N(N-1)}{2}, \tag{29}$$

$$[I(\theta)]_{31} = [I(\theta)]_{13} = 0, \tag{30}$$

$$[I(\theta)]_{32} = [I(\theta)]_{23} \approx \frac{\pi A^2}{\sigma^2}\frac{N(N-1)}{2}, \tag{31}$$

$$[I(\theta)]_{33} = \frac{1}{\sigma^2}\sum_{n=0}^{N-1} A\sin(\alpha)\times A\sin(\alpha) = \frac{A^2}{\sigma^2}\sum_{n=0}^{N-1}(\frac{1}{2}-\frac{\cos 2\alpha}{2}) \approx \frac{NA^2}{2\sigma^2}, \tag{32}$$

Above all, the Fisher Information Matrix is:

$$I(\theta)=\begin{bmatrix} \frac{N}{2\sigma^2} & 0 & 0 \\ 0 & \frac{(2\pi A)^2}{2\sigma^2}\frac{N(N-1)(2N-1)}{6} & \frac{\pi A^2}{\sigma^2}\frac{N(N-1)}{2} \\ 0 & \frac{\pi A^2}{\sigma^2}\frac{N(N-1)}{2} & \frac{A^2 N}{2\sigma^2} \end{bmatrix}. \tag{33}$$

To calculate the inversion of the Fisher Information Matrix:

$$[I(\theta)]_{22}^{-1}=\frac{\frac{A^2N^2}{4\sigma^4}}{\frac{\pi^2A^4N^3(N^2-1)}{24\sigma^6}}=\frac{3}{\pi^2\times SIR\times N(N^2-1)}, \tag{34}$$

where SIR is the signal to interference ratio, which is $\frac{A^2}{2\sigma^2}$.

And the CRLB for f_0 is:

$$\text{var}(\hat{f}_0)\geq\frac{3}{\pi^2\times SIR\times N(N^2-1)}. \tag{35}$$

Besides,

$$f_0=\frac{f_b}{f_s},T=\frac{1}{f_s}N, \tag{36}$$

$$f_b=f_1-f_2=S\frac{2r}{c}=\frac{W}{T}\frac{2r}{c}=\frac{W}{\frac{1}{f_s}N}\frac{2r}{c}=\frac{f_sW}{N}\frac{2r}{c}, \tag{37}$$

where S is the slope of the chirp, r is the distance between the radar and the target, c is the speed of light, W is the bandwidth, T is the duration for the frequency of the chirp increases from the lower bound to the higher bound such as from 60 GHz to 64 GHz.

Therefore, we can get

$$f_0=\frac{2rS}{f_Sc}, \tag{38}$$

$$\mathrm{var}(f_0) = \frac{4S^2}{f_S{}^2 c^2}\mathrm{var}(r), \tag{39}$$

$$\begin{aligned}\mathrm{var}(r) &\geq \frac{f_S^2 c^2}{4S^2}\frac{3}{\pi^2 \times SIR \times N(N^2-1)} \\ &= \frac{f_S^2 c^2}{4(\frac{W}{T})^2}\frac{3}{\pi^2 \times SIR \times N(N^2-1)} \\ &= \frac{3N^2 c^2}{4\pi^2 \times SIR \times W^2 N(N^2-1)} \approx \frac{3c^2}{4\pi^2 \times SIR \times NW^2}.\end{aligned} \tag{40}$$

3.1.4 A Testbed for Measurement of the SINR

Fig. 3 shows the basic scenario for empirical measurement of the received signal at the radar from the IEEE 802.11ad as an object close to the radar when the IEEE 802.11ad is on and off. When it is off the received signal at the radar is P_S. In this scenario, we measure the distances between the target and the mmWave radar as *d*. In addition, when the IEEE 802.11ad is on, we can measure P_I. In this scenario, we measure the distance between the interference source and mmWave radar, *r*, and AOA, α.

The testbed is built in a laboratory environment. As shown in Fig. 3.4, TX and RX are set apart for 7.5 meters. To measure P_S, the TX and RX are turned off, the TX is set as the target, the distance between radar and target, *r*, is changed from 0.6m to 2.1m. To measure P_I, the TX and RX are turned on, the TX is set as the interference source, the distance between radar and TX, *r*, is changed from 0.7m to 2.2m, and in each location, the radar is rotated to make AOA, α, equals to 0, 30, and 60 degrees separately.

The frame rate of the radar is set as 10 frames per second, the range resolution is set as 0.044 meters, the maximum unambiguous range is set as 9.02 meters, and the maximum radial velocity is set as 1 meter per second. The software used to detect the object is mmWave Demo Visualizer 3.5, provided by Texas Instruments. It uses the Constant false alarm rate (CFAR) algorithm to detect the object. The radar uses this software to plot the relative RSSI for different objects with different distances. The received power and distances of the objects can be used for modeling the

received signal strength indicator (RSSI). In this software, people can set parameters such as the number of frames per second, the threshold for the algorithm to detect the object, etc., and read the relative power and the distance of the target.

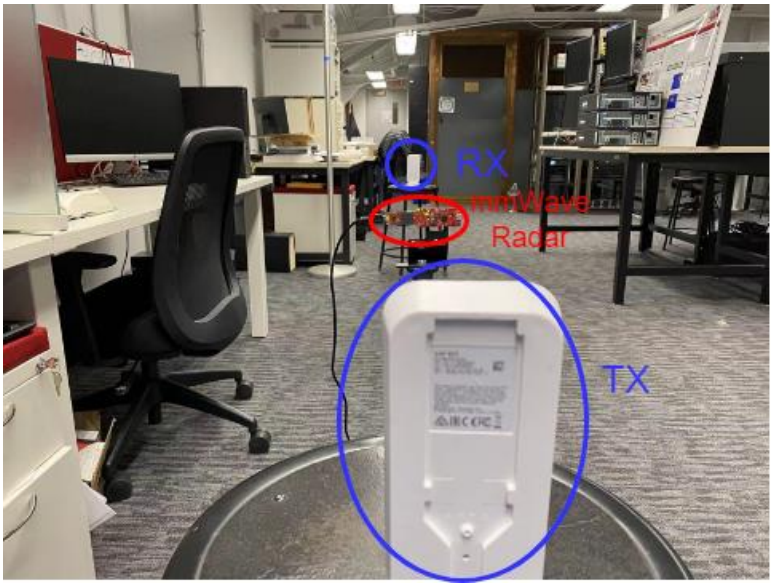

(a)

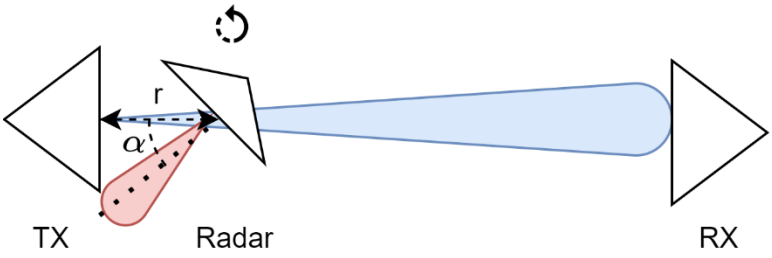

(b)

Figure 3. 4: Scenario for the IEEE 802.11ad communication link interference to TI mmWave radar a) The IEEE 802.11ad TX is set as the interference source and detected target for the radar, The distance between IEEE 802.11ad TX and RX is fixed as 7.5 meters. The distance between the IEEE 802.11ad TX and radar is *r*. b) When the TX is turned off, we move the radar away from the TX to measure the P_S ; When the TX is turned on, we move the radar away from the TX and rotate the radar to make the interference signal from IEEE 802.11ad TX has different angle of arrival, and measure the P_I .

Fig. 3.5(a) shows the results received by mmWave Demo Visualizer that is accessible in [12] . The blue line represents the power of the signal, the green line represents the noise floor, and the yellow points represent the detected objects. It is shown that when the IEEE 802.11ad communication is turned off, the radar can detect multiple objects with different distances. Fig. 3.5(b) shows that when the IEEE 802.11ad communication is turned on, it reduces the SINR of strong targets and buries week targets.

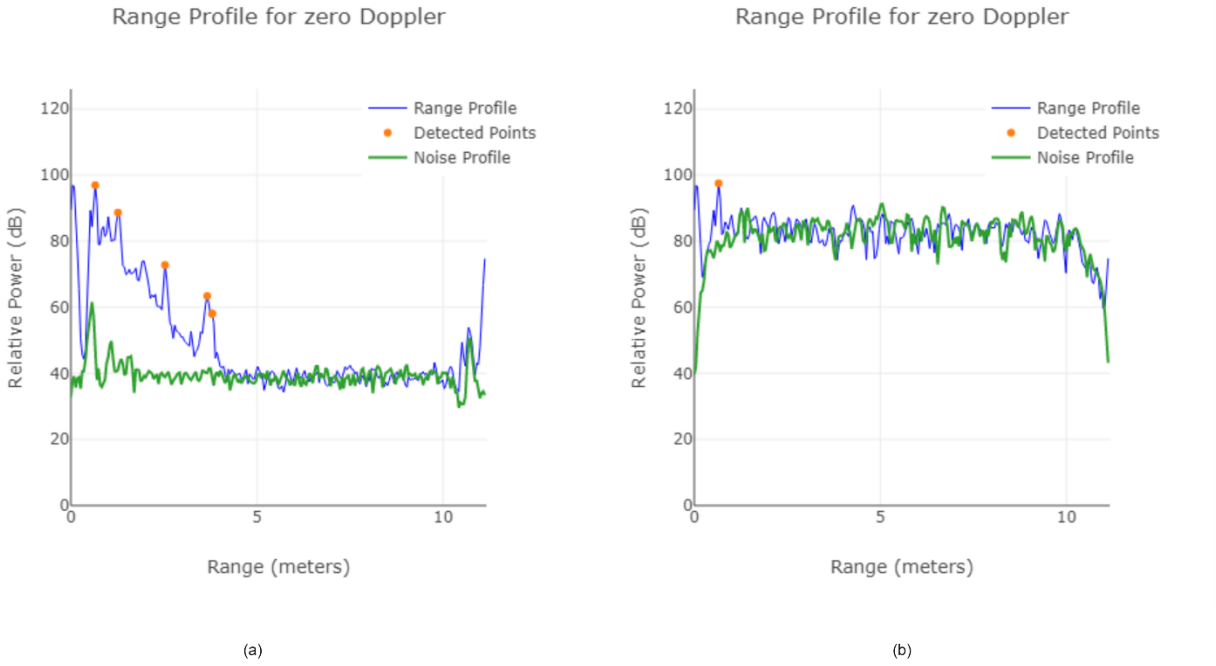

Figure 3. 5: Relative power of the detected objects a) turn off the IEEE 802.11ad communication, b) turn on the IEEE 802.11ad communication.

3.2. mmWave radar interference to IEEE 802.11ad

3.2.1 Introduction

The interference applied by mmWave radar to IEEE 802.11ad causes packet losses. Indeed, when the radar is on and operates in the same band as the IEEE 802.11ad the transmitted packets will be corrupted, and the packets will be counted as lost packets. As a result, we can establish a timing diagram to calculate the theoretical PLR caused by interference from the mmWave radar. To validate these results, we need a testbed to measure the packet loss rate. In this section, we first present a theoretical foundation for calculation of the effects of mmWave radar interference

on PLR of the IEEE 802.11ad, then we introduce a testbed for validation of the theoretical foundation.

3.2.2 A Theoretical Foundation for Interference of Radar into IEEE802.11ad

In this paper, the IEEE 802.11ad device works on the SC mode, the center frequency is 62.64 GHz, and the bandwidth is 2.16 GHz. The TI mmWave radar is working on the band from 60 GHz to 64 GHz. The interference time ratio model is introduced to analyze the interference between FMCW radar and communication [19] . The interference time ratio model is shown in Fig. 7. B_c represents the bandwidth of the IEEE 802.11ad communication, B_r is the bandwidth of mmWave radar. For the radar, every frame has 48 chirps, ramp end time is the sweep time for one chirp. Between each chirp, it has an inter-chirp idle time, and between each frame, it has an inter-frame idle time.

The interference time ratio is the time ratio in one frame that the frequency bands of mmWave radar and IEEE 802.11ad communication are overlapped. As the radar is set close to the RX of IEEE 802.11ad communication, the power of interference is very high compared to the RSSI of the communication signal. Assume when their frequency bands are overlapped, the packets will get lost, the packet loss rate (PLR) is approximately equal to the interference time ratio.

$$PLR \approx \frac{\frac{B_c}{B_r} N_c}{t_f} = \frac{\frac{B_c}{B_r} N_c}{\frac{1}{r_f}}, \tag{41}$$

where B_c is the bandwidth of IEEE 802.11ad, B_r is the bandwidth of mmWave radar, N_c is the number of chirps in one frame, t_f is the duration of the frame, and r_f is the frame rate.

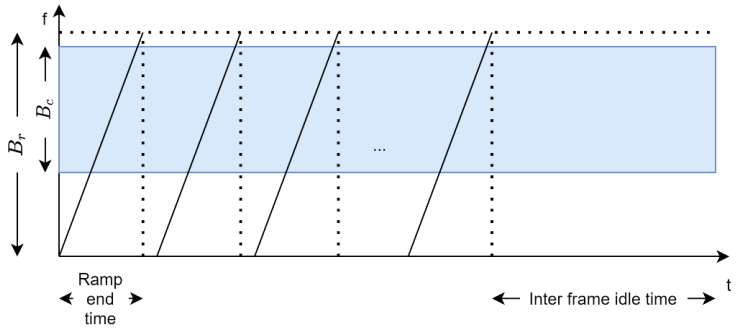

Figure 3. 6: The sawtooth waveform of the millimeter-wave radar occupies B_r bandwidth and IEEE 802.11ad occupies B_c bandwidth. When their frequencies overlapped with each other, IEEE 802.11ad gets interference from the radar signal.

Chapter 4

4. Results

In this section, the experimental results will be used to compared with the theoretical results to prove the analysis mentioned in the previous sections. When consider IEEE 802.11ad interferes to mmWave radar system, the change of coverage and accuracy of TI mmWave radar system is used to prove of the interference. When mmWave radar system interferes to IEEE 802.11ad communication system, the packet loss rate is used to prove the existence of the interference.

4.1 IEEE 802.11ad interference to mmWave radar

In this section, the RSS model is built in different scenarios. When we analyze the interference on the coverage of radar system, we consider the change of the SINR at the receiver because radar system detects objects based on the SINR. Besides, when we consider the change of accuracy of radar system, we use CRLB to compare the theoretical distance measurement error (DME) and range resolution of the system to check the change of accuracy.

4.1.1 An Empirical Models for SIR

a) In CWINS lab scenario

In the tests conducted in the laboratory, the detected object is TX, therefore, the RCS is fixed in the experiment. The P_S model in dB is shown in Fig. 4.1. Here, the path loss exponent is set as 4, the theoretical value in (14). The model is:

$$P_s(dB) = -40\log_{10} r + 101.7 \tag{42}$$

, where r is the distance between the radar and a target. In this model, the mean value of the shadow fading is -0.04 dB, the standard deviation of the shadow fading is 3.78 dB.

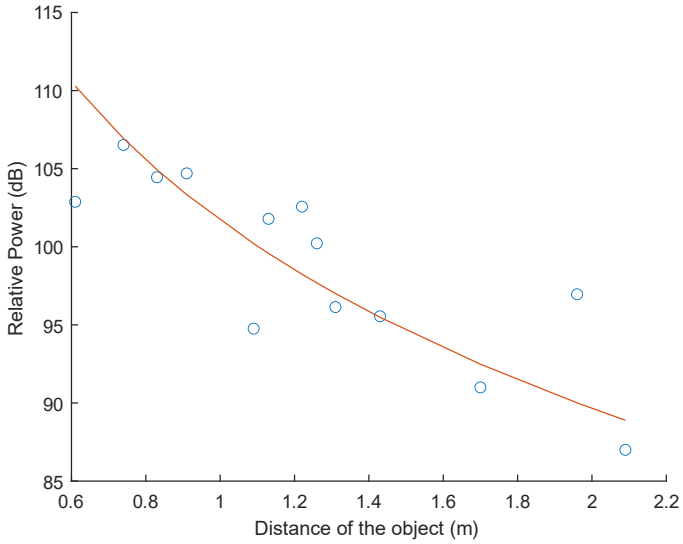

Figure 4. 1: Power of signal model in the laboratory scenario

In our laboratory tests, the radar is moved away from the RX and rotated to make AOA, α, equals 0, 30, and 60 degrees respectively as shown in Fig. 4.2. The P_I model in dB is shown in Fig. 6. Based on (15), the interference path loss exponent will be 2, and based on Fig. 6 the overall interference path loss model is:

$$P_I(dB) = -20\log_{10}(r) + 22\log10(\cos(\alpha)) + 73.06 \quad (43)$$

, where r is the distance between the radar and the TX, and α is AOA, which is in the range from -60 degrees to 60 degrees because of the field of view of the radar. In this model, the mean value of the shadow fading is 0.004 dB, the standard deviation of the shadow fading is 1.07 dB. In (7), the coefficient of $\cos(\alpha)$ represents the relationship between AOA and the antenna gain of RX, which is modeled based on the datasheet of IWR6843AOPEVM radar [34] .

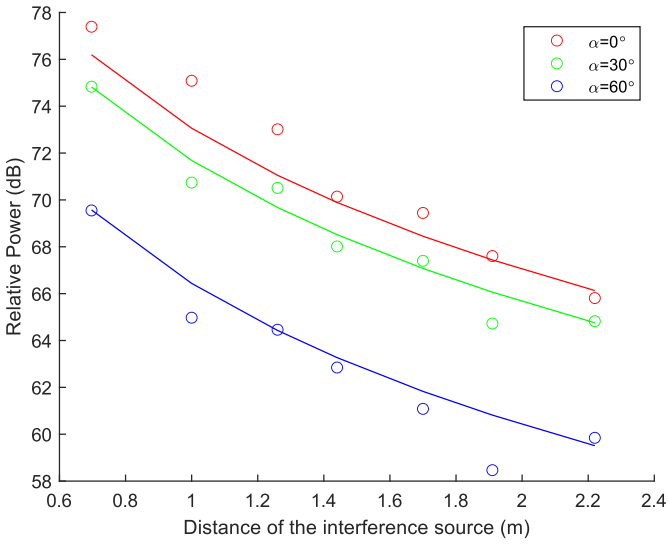

Figure 4. 2: Power of interference model in the laboratory scenario

The SINR is calculated from (16), based on the P_S model and P_I model. As the typical SNR value requirement for detecting the target is from 15dB to 20dB. We assume the SNR that is needed to detect the object is 20dB and analyze the influence of the range the radar can detect when the IEEE 802.11ad communication is introduced. Fig. 4.3 shows the SIR model. When the interference source is close to the radar, the detection range decreases significantly.

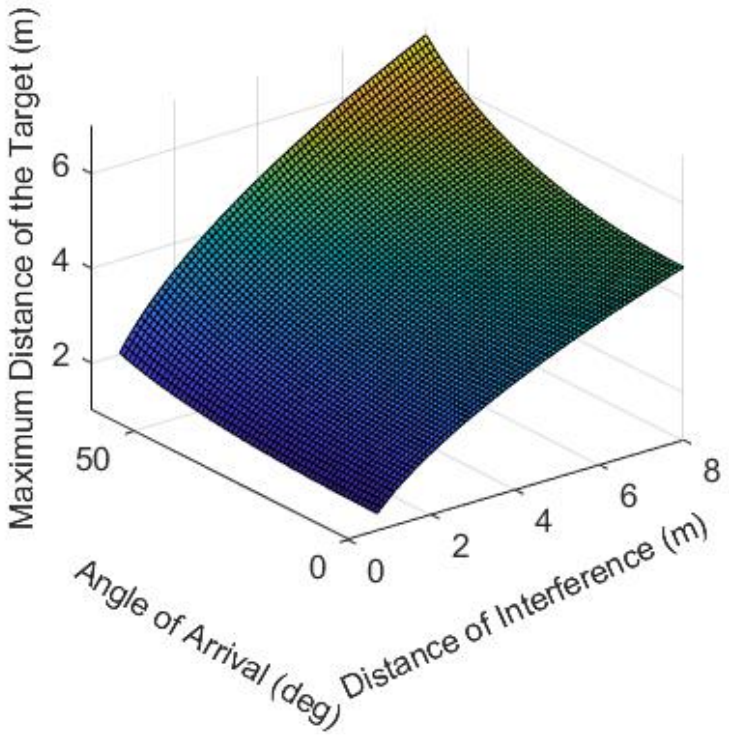

Figure 4. 3: The coverage of the mmWave radar under the IEEE 802.11ad communication when the SIR is 20dB

As shown in Fig 4.3, when we introduce the interference source, the IEEE 802.11ad communication system, the coverage of the TI mmWave radar will decrease. The reason is the value of the SINR needed for mmWave radar system to detect objects is fixed at 20 dB. As the IEEE 802.11ad transmitter moved toward to the TI mmWave radar, the power of the interference increased, however, the power of the signal is fixed because the object did not move, as a result, the SINR decreased. When the IEEE 802.11ad transmitter is close enough to make the SINR less than 20dB, even the objects did not move, some of them would not be detected. Above all, coverage of the mmWave radar decrease significantly because of the introduction of the IEEE 802.11ad system.

Besides, from Fig. 4.3, we can also find that, when the distance between the IEEE 802.11ad transmitter and radar was fixed, as we changed the AOA, the coverage of radar system would also change. This is because when the AOA changes, the antenna gain of the receiver also changes based on the antenna pattern mentioned in the datasheet of the TI mmWave radar. When the AOA is 0 degree, which means the interference signal is vertical to the receiver of mmWave radar, the mmWave radar system will get the highest power of interference with the fixed distance between

IEEE 802.11ad transmitter and mmWave radar. As we rotated the mmWave radar, the antenna gain of the receiver decreased, and the power of interference received by the radar decreased, therefore, the SINR increased. As a result, when the distance between radar and IEEE 802.11ad transmitter is fixed, with the increasing of AOA, the coverage of the TI mmWave radar increases because of the increasing of SINR.

b) In the corridor scenario

In the corridor scenario, the ceiling, floor, and the walls perform like a waveguide, therefore, the power gradient is less than 4. According to the linear regression, the P_S model is as follows:

$$P_S = -10.68 \times \log_{10} r + 100.9, \tag{44}$$

where r is the distance between the object and mmWave radar. The mean value of the shadow fading is 0.0019 dB, the standard deviation of the shadow fading is 1.34 dB. The P_S model in dB is shown in Fig. 4.4.

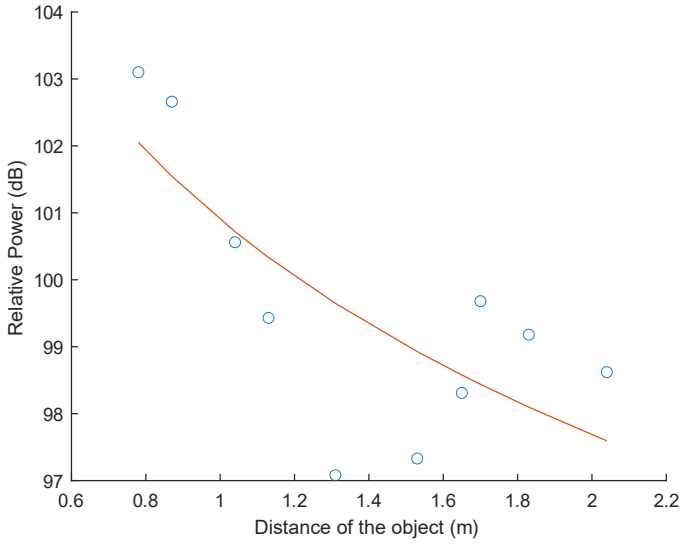

Figure 4. 4: Power of signal model in the corridor scenario

In our corridor scenario, the radar is moved away from the RX and rotated to make AOA, α, equals 0, 30, and 60 degrees respectively. The interference path loss exponent will be less than 2, because of the reflection in this scenario, as shown in Fig. 4.5, the overall interference path loss model is:

$$P_I(dB) = -12.56\log_{10}(r) + 22\log10(\cos(\alpha)) + 71.68, \tag{45}$$

where r is the distance between the radar and the TX, and α is AOA, which is in the range from -60 degrees to 60 degrees. In this model, the mean value of the shadow fading is 0.0171 dB, the standard deviation of the shadow fading is 2.15 dB. In (45), the coefficient of $\cos(\alpha)$ represents the relationship between AOA and the antenna gain of RX.

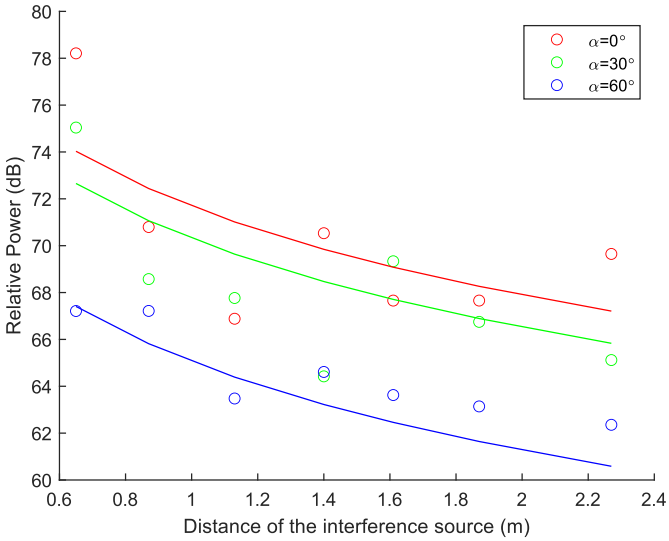

Figure 4. 5: Power of interference model in the corridor scenario

The SINR is calculated from (16), based on the P_S model and P_I model. We assume the SNR that is needed to detect the object is 20dB and analyze the influence of the range the radar can detect when the IEEE 802.11ad communication is introduced. Fig. 4.6 shows the SIR model. When the interference source is close to the radar, the detection range does not decrease significantly.

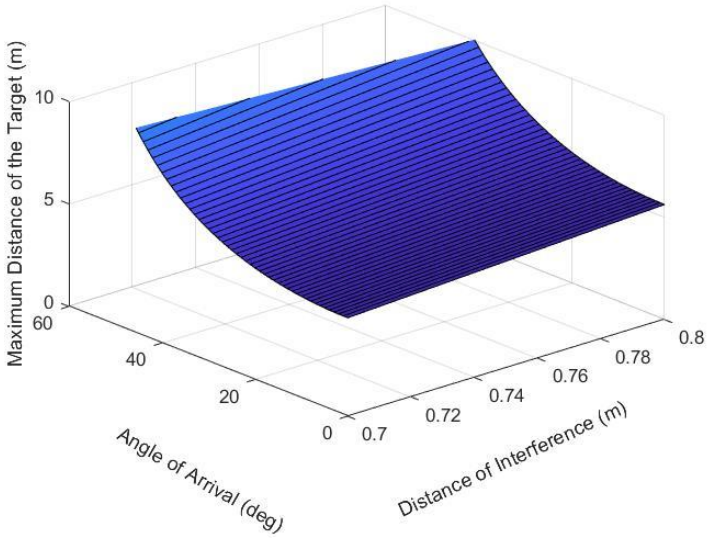

Figure 4. 6: The coverage of the mmWave radar under the IEEE 802.11ad communication when the SIR is 20dB

In this scenario, as shown in Fig. 4.6, the coverage of the radar is not influenced significantly because of the introduction of IEEE 802.11ad communication system. Only when the AOA is around 0 degree and the distance between the radar and IEEE 802.11ad transmitter is very close, the coverage of mmWave radar will decrease. This is because in the corridor scenario, the power gradient is less than that in the laboratory scenario, the path loss of the signal power is less than that in the laboratory scenario as well. According to the experimental results, the power gradients of the signal power reflected from object and interference power sent by IEEE 802.11ad are close, therefore, to get a lower SINR, we have to put the IEEE 802.11ad transmitter very close to the mmWave radar because the power of the signal is very high in this scenario.

4.1.2 CRLB for Precision of the Radar

To analyze the influence of the accuracy of the radar, we use Cramer–Rao lower bound (CRLB). Even though, the TI mmWave radar detect the object based on the frequency of IF signal, when the power of the interference is very high, the system may also get distance measurement error because the peak of the power with different frequency may change. In classical estimation theory, ranging and positioning are estimated based on single or multiple parameters, and CRLB is a mean for the calculation of the variance of those parameters [31] . In [35] [36] , the CRLB of the FMCW radar can be calculated as follows:

Firstly, after the mixture of transmitted signal and received signal, the IF signal is:

$$x_{IF}(t) = A\sin(2\pi f_b t + \varphi_b), \tag{46}$$

where A is the amplitude of the IF signal, the phase is φ_b, and the frequency of the IF signal is f_b.

The frequency of IF signal is related to the target distance:

$$f_b = \frac{W}{T}\frac{2r}{c}, \tag{47}$$

where W is the bandwidth, T is the sweep time, the distance between target and radar is r, and the speed of light is c. As the sampling frequency is a discrete process:

$$\frac{f_b}{f_s} = \frac{W}{N}\frac{2r}{c}, \tag{48}$$

where f_s is the sampling frequency, N is the number of samples taken in observation window T. As we assume the interference power is distributed as white gaussian noise, we can get:

$$\mathrm{var}\left\{\frac{f_b}{f_s}\right\} \geq \frac{12}{(2\pi)^2 \times SNR \times N(N^2-1)}. \tag{49}$$

We can also get equation from (49) that:

$$\mathrm{var}\left\{\frac{f_b}{f_s}\right\} = \frac{4W^2}{N^2c^2}\mathrm{var}\{r\} \tag{50}$$

Therefore, we can get new equation based on (50) and (51) that:

$$CRLB = \mathrm{var}(r) \geq \frac{3c^2}{(2\pi)^2 \times SNR \times NW^2}, \tag{51}$$

where c is the speed of light, SNR is the signal to the noise ratio, N is the number of samples taken in the observation window, W is the bandwidth of the radar. In this scenario, we assume the distribution of the IEEE 802.11ad communication signal is the same as the thermal noise. The power of the thermal noise is neglected because it is far less than the power of interference. Therefore, when the interference is introduced, the CRLB is:

$$CRLB = \mathrm{var}(r) \geq \frac{3c^2}{(2\pi)^2 \times SIR \times NW^2} \tag{52}$$

The distance measurement error (DME) is:

$$DME = \sqrt{CRLB} \tag{53}$$

Given SNR for object detection is 20dB, the CRLB and the DME can be calculated using (53) and (54), respectively. As shown in (11), R_{res} of FMCW radar is independent of SNR and therefore interference doesn't change the range resolution. Based on the set parameters, range resolution is in the order of 0.04m, while the DME reduces with SNR, and it is in the order of 10^{-4}m. Thus, DME is much less than range resolution and the impact of interference on range estimation would not be detectable. In the experiment, when we introduced the IEEE 802.11ad communication system as interference source, the position of those detected objects did not change.

4.2. mmWave radar interference to IEEE 802.11ad

In this section, we measure the packet loss rate of the IEEE 802.11ad communication system when the mmWave radar system is introduced in CWINS lab scenario. The experimental results are compared with those theoretical results to prove the existence of interference. According to the results we have got, the PLR will increase when the mmWave radar is introduced, which means the quality of communication system will decrease as a result.

4.2.1 Empirical PLR for Validation of the Theoretical Foundation

In this scenario, as is shown in Fig. 4.7, the IEEE 802.11ad TX and RX are set 3.6 meters apart in the laboratory. The distance between the radar and RX is 40 cm. The frame rate of the radar is changed from 10 frames per second to 30 frames per second. The ramp end time for every chirp is 200 μs, the inter-chirp idle time is 8 μs, the number of chirps in one frame is 48. For the IEEE 802.11ad communication, the payload of the packet is set as 6000 Bytes, and the packet loss rate is measured under the UDP protocol. The software Iperf3 was used to measure the packet loss rate. The measurement time is 30 seconds, and the average value of 10 measurements is the experimental result in this experiment. When the interference is not introduced, the analytical result of the packet loss rate is 0, the experimental result of the packet loss rate is 0.0579%. Table 4.1 shows the analytical and experimental packet loss rates when we introduced the interference based on different frame rates. Fig. 4.8 shows

the relation between the packet loss rate and the frame rate of the radar. The experimental results are distributed around the analytical results.

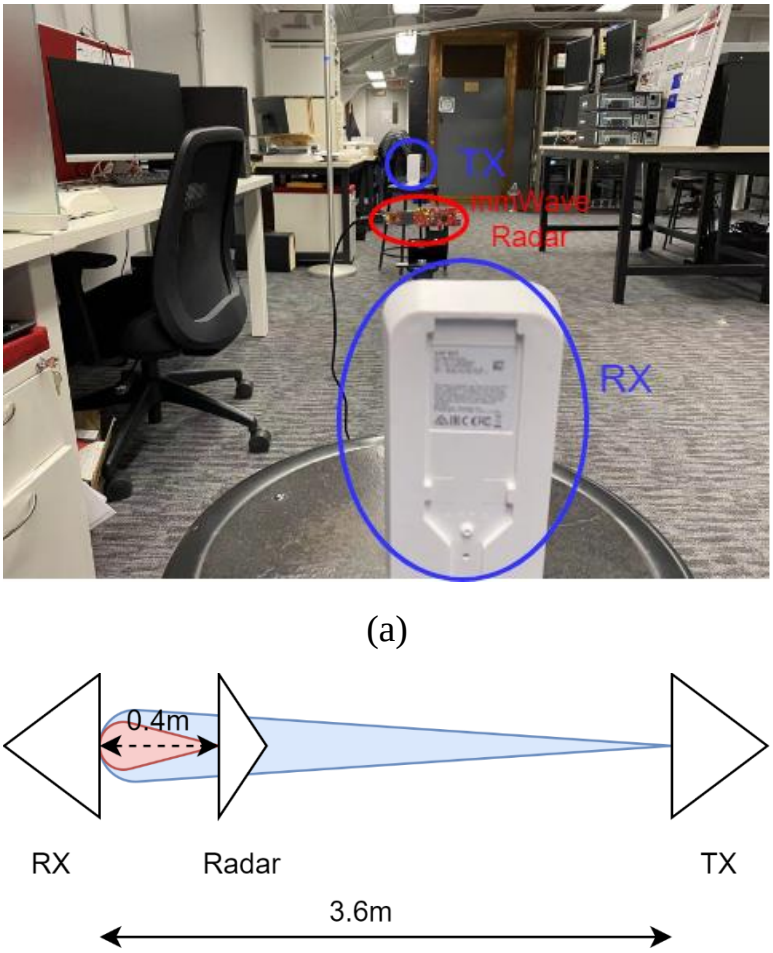

Figure 4. 7: Scenario for the TI mmWave radar interference to the IEEE 802.11ad communication link a) The testbed setting in CWINS lab scenario b) The distance between TX and RX is 3.6 meters, and the distance between the radar and the RX is 0.4 meters.

Table 4. 1: Analytical and experimental packet loss rates of the IEEE 802.11ad communication based on different configurations of mmWave radar

Frames per second	Ramp end time (μs)	Inter-chirp idle time (μs)	Inter-frame idle time (ms)	Packet loss rate (Analytical)	Packet loss rate (Experiment)
10	200	8	90.02	5.18%	3.23%
15	200	8	56.68	7.78%	6.58%
20	200	8	40.02	10.37%	8.60%
25	200	8	30.02	12.96%	13.42%
30	200	8	23.35	15.55%	18%

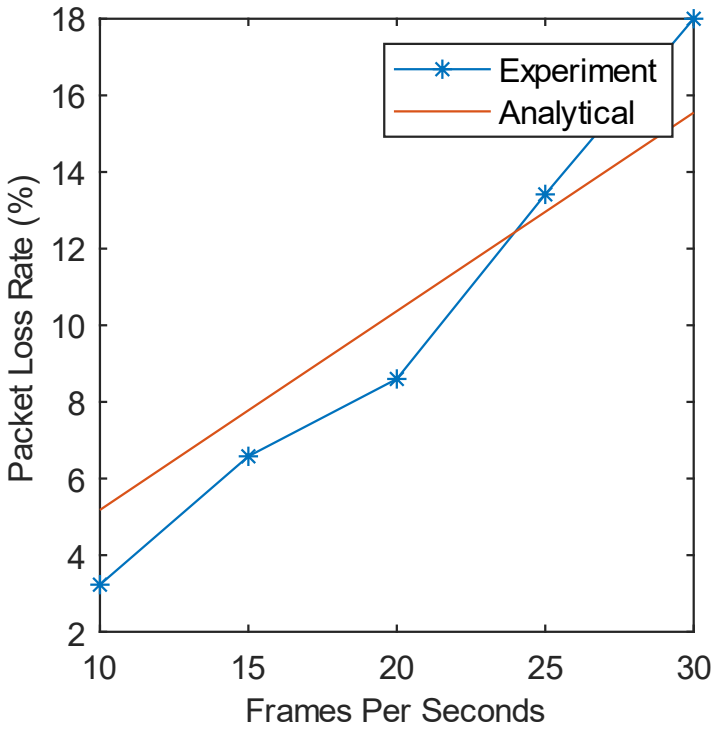

Figure 4. 8: Analytical and experimental results of the IEEE 802.11ad packet loss rate under the interference from mmWave radar at different frame rates.

As shown in Fig. 4.8, with the increasing of the frames per second, the time ratio when the frequency band of mmWave radar and IEEE 802.11ad are overlapped increases, therefore, the interference time ratio increases. According to the analysis mentioned in section 3.2.2, the PLR increases when the interference time ratio increases. In Fig. 4.8, the experimental results are distributed around the theoretical results, which can prove the existence of the interference.

Chapter 5

5. Conclusion and Future Work

In this thesis, the interference between IEEE 802.11ad and mmWave radar is analyzed. To analyze IEEE 802.11ad interference to mmWave radar, we build the P_S and P_I model of the radar within the laboratory and corridor environments and use SINR and CRLB to explain the influence on the range and the accuracy on the radar performance. In the CWINS lab scenario, as the RCS of the object is fixed, when the interference from IEEE 802.11ad communication is introduced, the detection range of the radar decreases. Specifically, when the distance between the IEEE 802.11ad TX and the mmWave radar is 0.4m with a 0-degree AOA, the detection range decreases from 9m to 1m. However, in the corridor scenario, the coverage of the radar is not influenced significantly. Only in the case when the radar is set close to the TX, the coverage of the radar system will decrease. For example, when the distance between the radar and the TX is 0.7 meters, the coverage of the radar system decreases from 9m to 4.8m. The accuracy for the detected objects will not change. To analyze the mmWave radar interference to IEEE 802.11ad communication, the interference time ratio model is introduced. When the frequency bands of IEEE 802.11ad and mmWave radar overlap, the IEEE 802.11ad communication will interfere. When the frame rate of the radar is increased from 10 frames per second to 30 frames per second, the theoretical ratio of time when the frequency bands of IEEE 802.11ad and radar overlap increased. As a result, the theoretical packet loss rate increases from around 5% to 15%. And the experimental results are close to the theoretical results. When the frame rate is 30 frames per second, the ramp end time is 200 μs , the packet loss rate increases up to 15%.

In the future work, we will set the testbed in different scenarios, such as open area, anechoic chamber, faraday cage, etc., to test the interference between mmWave radar and IEEE 802.11ad. The mitigation techniques which are used to improve the performance of mmWave radar and IEEE 802.11ad systems under interference should be analyzed in different scenarios to fully understand isolated and combined effect of various environmental parameters such as reflection and scattering.

References

[1] K. Pahlavan and P. Krishnamurthy, “Evolution and Impact of Wi-Fi Technology and Applications: A Historical Perspective,” *International Journal of Wireless Information Networks*, vol. 28, pp. 3–19, Mar 2021.

[2] K. Pahlavan, "Wireless communications for office information networks," in *IEEE Communications Magazine*, vol. 23, no. 6, pp. 19-27, June 1985, doi: 10.1109/MCOM.1985.1092598.

[3] K. Pahlavan, Wireless intra-office networks, *ACM Transactions on Information Systems (TOIS)*, Vol. 6, No. 3, pp. 277–302, 1988.

[4] K. Pahlavan, J. Ying, Z. Li, E. Solovey, J. P. Loftus and Z. Dong, "RF Cloud for Cyberspace Intelligence," in *IEEE Access*, vol. 8, pp. 89976-89987, 2020, doi: 10.1109/ACCESS.2020.2993548.

[5] T. M. Siep, I. C. Gifford, R. C. Braley and R. F. Heile, "Paving the way for personal area network standards: an overview of the IEEE P802.15 Working Group for Wireless Personal Area Networks," in *IEEE Personal Communications*, vol. 7, no. 1, pp. 37-43, Feb. 2000, doi: 10.1109/98.824574.

[6] United States radio spectrum frequency allocations chart as of January 2016, [Online] Available: https://www.ntia.doc.gov/files/ntia/publications/january_2016_spectrum_wall_chart.pdf

[7] BEST-NEST Invitational Online Workshop on “New Paradigms in Intelligent Spectrum Management and Regulations, Future Directions, Technologies, Standards, and Applications”, Dec 3-4, 2020, Webinar from WPI, Worcester, MA (https://bestnest.wpi.edu/index.php/synapsis-2/)

[8] C. Iovescu and S. Rao, ‘‘The fundamentals of millimeter wave sensors,’’ Texas Instrum., Dallas, TX, USA, Tech. Rep., 2017, pp. 1–8.

[9] S. Cheng, K. Pahlavan, H. Wei, Z. Su, S. A. Zekavat, A. Abedi, “A Study of Interference Analysis Between mmWave Radars and IEEE 802.11AD at 60GHz Bands” Accepted by International Journal of Wireless Information Networks (IJWIN), 2022

[10] T. Nitsche, C. Cordeiro, A. B. Flores, E. W. Knightly, E. Perahia and J. C. Widmer, "IEEE 802.11ad: directional 60 GHz communication for multi-Gigabit-per-second Wi-Fi [Invited Paper]," in *IEEE Communications Magazine*, vol. 52, no. 12, pp. 132-141, December 2014, doi: 10.1109/MCOM.2014.6979964.

[11] J. Kim, S. -C. Kwon and G. Choi, "Performance of Video Streaming in Infrastructure-to-Vehicle Telematic Platforms With 60-GHz Radiation and IEEE 802.11ad Baseband," in *IEEE Transactions on Vehicular Technology*, vol. 65, no. 12, pp. 10111-10115, Dec. 2016, doi: 10.1109/TVT.2016.2547943.

[12] M. V. S. Chandrashekhar, P. Choi, K. Maver, R. Sieber and K. Pahlavan, "Evaluation of interference between IEEE 802.11b and Bluetooth in a typical office environment," *12th IEEE International Symposium on Personal, Indoor and Mobile Radio Communications. PIMRC 2001. Proceedings (Cat. No.01TH8598)*, 2001, pp. D-D, doi: 10.1109/PIMRC.2001.965494.

[13] F. H. Sanders, R. L. Sole, J. E. Carroll, G. S. Secrest, and T. L. Allmon, "Analysis and resolution of RF interference to radars operating in the band 2700-2900 MHz from broadband communication transmitters," *U.S. Dept. Commerce, Nat. Telecommun. Inform. Admin., NTIA Report 13-490*, 2012

[14] K. Pahlavan and P. Krishnamurthy, *Networking fundamentals: wide, local and personal area communications*. John Wiley & Sons, 2009.

[15] F. R. Gfeller and U. Bapst, "Wireless in-house data communication via diffuse infrared radiation," in *Proceedings of the IEEE*, vol. 67, no. 11, pp. 1474-1486, Nov. 1979, doi: 10.1109/PROC.1979.11508.

[16] P. Freret, R. Eschenbach, D. Crawford and P. Braisted, Applications of spread-spectrum radio to wireless terminal communications, *Proceedings of the IEEE NTC*, Vol. 4, pp. 244–248, 1980

[17] Abramson, N., 1970, November. THE ALOHA SYSTEM: another alternative for computer communications. In *Proceedings of the November 17-19, 1970, fall joint computer conference* (pp. 281-285).

[18] V. Deniau, C. Gransart, G. L. Romero, E. P. Simon and J. Farah, "IEEE 802.11n Communications in the Presence of Frequency-Sweeping Interference Signals," in *IEEE Transactions on Electromagnetic Compatibility*, vol. 59, no. 5, pp. 1625-1633, Oct. 2017, doi: 10.1109/TEMC.2017.2684428.

[19] C. Aydogdu, M. F. Keskin, N. Garcia, H. Wymeersch and D. W. Bliss, "RadChat: Spectrum Sharing for Automotive Radar Interference Mitigation," in *IEEE Transactions on Intelligent Transportation Systems*, vol. 22, no. 1, pp. 416-429, Jan. 2021, doi: 10.1109/TITS.2019.2959881.

[20] Z. Yang and A. Mani, "Interference mitigation for AWR/IWR devices," Texas Instrument, Dallas, TX, USA, 2020.

[21] T. Yamawaki and S. Yamano, “60-GHz millimeter-wave automotive radar,” Fujitsu Tech. Rev., vol. 15, no. 2, pp. 9–18, 1998

[22] P. Kumari, N. Gonzalez-Prelcic and R. W. Heath, "Investigating the IEEE 802.11ad Standard for Millimeter Wave Automotive Radar," *2015 IEEE 82nd Vehicular Technology Conference (VTC2015-Fall)*, 2015, pp. 1-5, doi: 10.1109/VTCFall.2015.7390996.

[23] S. Rangan, T. S. Rappaport and E. Erkip, "Millimeter-Wave Cellular Wireless Networks: Potentials and Challenges," in *Proceedings of the IEEE*, vol. 102, no. 3, pp. 366-385, March 2014, doi: 10.1109/JPROC.2014.2299397.

[24] P. Smulders, "Exploiting the 60 GHz band for local wireless multimedia access: prospects and future directions," in *IEEE Communications Magazine*, vol. 40, no. 1, pp. 140-147, Jan. 2002, doi: 10.1109/35.978061.

[25] Hao Xu, V. Kukshya and T. S. Rappaport, "Spatial and temporal characteristics of 60-GHz indoor channels," in *IEEE Journal on Selected Areas in Communications*, vol. 20, no. 3, pp. 620-630, April 2002, doi: 10.1109/49.995521.

[26] IEEE Standard for Information Technology-Telecommunications and Information Exchange Between Systems-Local and Metropolitan Area Networks-Specific Requirements-Part 11: Wireless LAN Medium Access Control (MAC) and Physical Layer (PHY) Specifications Amendment 3: Enhancements for Very High Throughput in the 60 GHz Band, IEEE Std. 802.11ad Spec., Dec. 2012.

[27] K. Ramasubramanian, Using a *Complex-Baseband Architecture in FMCW Radar Systems*. Dallas, TX, USA: Texas Instruments, 2017. [Online]. Available: https://www.ti.com/lit/wp/spyy007/spyy007.pdf

[28] T. Instruments, mmWave Demo Visualizer Application., [online] Available: https://dev.ti.com/gallery/view/mmwave/mmWave_Demo_Visualizer/ver/3.5.0/ (accessed on 31 July 2021).

[29] “Iperf”. [Online]. Available: https://iperf.fr/

[30] S. Srivastava, S. Anmulwar, A. M. Sapkal, T. Batra, A. K. Gupta and V. Kumar, "Comparative study of various traffic generator tools," *2014 Recent Advances in Engineering and Computational Sciences (RAECS)*, 2014, pp. 1-6, doi: 10.1109/RAECS.2014.6799557.

[31] K. Pahlavan, *Indoor Geolocation Science and Technology*. Copenhagen, Denmark: River Publishers, 2019.

[32] A. Antonucci et al., "Performance Analysis of a 60-GHz Radar for Indoor Positioning and Tracking," *2019 International Conference on Indoor Positioning and Indoor Navigation (IPIN)*, 2019, pp. 1-7, doi: 10.1109/IPIN.2019.8911764.

[33] K. Pahlavan and A. H. Levesque, *Wireless Information Networks*, vol. 93. Hoboken, NJ, USA: Wiley, 2005.

[34] IWR6843AOPEVM Datasheet., [online] Available: https://www.ti.com/lit/pdf/swrs237 (accessed on 31 August 2021).

[35] S. M. Kay, *Fundamentals of Statistical Signal Processing: Estimation Theory*. Upper Saddle River, NJ, USA: Prentice-Hall, 1993.

[36] S. Scherr, S. Ayhan, M. Pauli and T. Zwick, "Accuracy limits of a K-band FMCW radar with phase evaluation," *2012 9th European Radar Conference*, 2012, pp. 246-249.

Appendix A

Selected Matlab Code

```
% ps and pi model in lab scenario
clear;clc;close all
d = [0.61 0.74 0.83 0.91 1.09 1.13 1.22 1.26 1.31 1.43
1.70 1.96 2.09 ];
d_log = 10*log10(d);
p = [102.88 106.52 104.45 104.70 94.76 101.79 102.57
100.22 96.14 95.55 91 96.96 87];

tiledlayout(1,2)
nexttile
disp('when alpha is 4.0')
disp('Mean value of shadow fading is:');
disp(mean(p-101.7+4.0*d_log));
disp('Standard Deviation of shadow fading is:');
disp(std(p-101.7+4.0*d_log));

scatter(d,p)
y = -4*10*log10(d) + 101.7;
hold on
plot(d,y)
xlim([0.6 2.4])
hold off
xlabel({'Distance of the object (m)';'(a)'})
ylabel('Relative Power (dB)')

nexttile
r = [0.697 1.00 1.26 1.44 1.70 1.91 2.22];
r_log = 10*log10(r);
% distance at 0.697 meters
p1(:,1) = [67.76 68.39 67.26 63.25 68.52 68.26 66.41
71.40 62.90 67.45]';
p1(:,2) = [72.28 73.09 74.32 73.85 73.34 71.99 71.43
75.04 72.84 76.42]';
p1(:,3) = [78.61 81.87 77.17 77.33 74.85 72.91 80.18
75.70 76.73 78.58]';
p1(:,4) = [73.44 75.63 77.58 78.68 78.05 80.12 78.77
74.32 75.01 70.46]';
```

```
p1(:,5) = [70.86 70.30 70.46 72.40 71.62 74.10 75.48
68.67 75.38 70.15]';
p_avg(1,:) = mean(p1);
% distance at 1.00 meters
p2(:,1) = [66.07 69.55 67.70 59.05 61.05 67.64 66.41
57.45 65.91 64.35]';
p2(:,2) = [69.93 70.02 74.03 71.71 67.83 65.22 68.70
63.93 71.65 67.07]';
p2(:,3) = [73.41 77.77 76.17 75.92 70.77 73.69 74.54
72.94 79.30 76.35]';
p2(:,4) = [73.94 72.91 74.00 70.68 75.63 77.01 77.26
66.45 69.99 66.85]';
p2(:,5) = [70.90 63.97 60.27 67.23 66.60 69.11 66.51
62.43 62.28 65.00]';
p_avg(2,:) = mean(p2);
% distance at 1.26 meters
p3(:,1) = [66.23 62.34 65.88 62.26 58.04 61.37 61.27
64.03 65.13 63.59]';
p3(:,2) = [71.65 69.21 69.55 69.61 71.34 67.76 66.85
67.67 64.94 73.72]';
p3(:,3) = [74.82 68.98 69.99 77.83 73.53 71.18 73.60
76.57 71.34 72.30]';
p3(:,4) = [75.00 69.30 66.57 74.79 68.52 74.19 74.72
72.28 70.05 72.56]';
p3(:,5) = [68.48 65.81 66.89 69.49 66.23 64.09 65.22
64.88 62.53 65.44]';
p_avg(3,:) = mean(p3);
% distance at 1.44 meters
p4(:,1) = [65.47 61.59 59.35 62.33 59.33 60.30 55.19
59.58 65.88 56.98]';
p4(:,2) = [62.62 61.43 63.18 67.36 65.69 64.25 70.15
68.89 64.22 67.32]';
p4(:,3) = [72.63 67.70 72.09 72.22 69.55 71.68 69.55
68.92 67.14 69.93]';
p4(:,4) = [75.29 72.81 70.24 63.27 71.18 73.28 71.02
71.15 68.86 68.07]';
p4(:,5) = [65.16 57.95 67.88 65.19 69.36 60.17 61.81
65.82 69.48 68.13]';
p_avg(4,:) = mean(p4);
% distance at 1.70 meters
```

```
p5(:,1) = [64.50 54.66 58.67 60.93 58.61 65.19 60.77
58.95 59.48 61.99]';
p5(:,2) = [66.85 68.58 72.44 66.03 61.65 64.91 69.08
68.77 66.32 62.55]';
p5(:,3) = [65.29 70.43 66.45 72.50 72.28 69.64 65.85
66.50 72.75 72.75]';
p5(:,4) = [67.64 68.83 70.30 73.56 60.49 68.36 69.74
62.59 66.76 72.56]';
p5(:,5) = [64.59 66.73 59.86 58.01 59.70 64.56 59.92
62.78 61.77 59.99]';
p_avg(5,:) = mean(p5);
% distance at 1.91 meters
p6(:,1) = [54.72 58.36 59.08 50.42 56.41 54.72 56.63
53.21 53.62 56.69]';
p6(:,2) = [60.74 56.35 63.03 65.16 62.46 68.52 67.54
69.30 57.44 62.40]';
p6(:,3) = [65.54 74.00 68.36 67.32 69.27 73.03 62.62
66.03 64.53 65.35]';
p6(:,4) = [68.08 62.59 68.45 70.71 63.06 67.51 63.09
64.82 68.89 64.38]';
p6(:,5) = [66.82 61.46 64.63 59.83 63.59 60.30 63.69
64.22 52.27 58.64]';
p_avg(6,:) = mean(p6);
% distance at 2.22 meters
p7(:,1) = [56.32 58.54 55.75 59.58 56.88 61.05 52.21
59.67 62.21 61.52]';
p7(:,2) = [70.02 67.01 56.69 61.81 60.39 58.14 70.99
62.50 65.94 60.49]';
p7(:,3) = [66.07 62.15 68.14 60.65 66.95 59.14 70.40
72.78 69.49 62.33]';
p7(:,4) = [67.92 59.74 68.74 68.98 70.71 68.74 66.70
60.80 64.56 65.63]';
p7(:,5) = [55.13 63.87 59.52 61.52 64.31 62.37 60.58
61.77 62.81 61.33]';
p_avg(7,:) = mean(p7);
% data processing
p60 = 0.5*(p_avg(:,1)+p_avg(:,5));
p30 = 0.5*(p_avg(:,2)+p_avg(:,4));
p0 = p_avg(:,3);
% liner fit
```

```
hold on
scatter(r,p0','r')
scatter(r,p30','g')
scatter(r,p60','b')
y0 = -20*log10(r)+22*log10(cos(0/180*pi))+73.06;
y30 = -20*log10(r)+22*log10(cos(30/180*pi))+73.06;
y60 = -20*log10(r)+22*log10(cos(60/180*pi))+73.06;
%%%%%%%

plot(r,y0,'r')
plot(r,y30,'g')
plot(r,y60,'b')

legend('\alpha=0\circ','\alpha=30\circ',...
    '\alpha=60\circ')
xlabel({'Distance of the interference source
(m)';'(b)'})
ylabel('Relative Power (dB)')
%title('P_I model in the laboratory scenario')
hold off
dme = [p0'-y0 p30'-y30 p60'-y60]';
mean(dme)
std(dme)
% antenna pattern curve fit
clear; clc; close all
angle = [-60:5:60];
G(1,:) = [-5.5 -4 -3 -2 -1.5 0 0 1 1.5 2 2 1 0 0 0 0 0
0 0 -1 -2 -3 -4 -4 -6];
G(2,:) = [-5.5 -4.5 -3.5 -2.5 -1.5 -0.5 0 1 1 1 0 0 0 0
0 0 0 0 0 -1.5 -2 -3 -4 -4 -6];
G(3,:) = [-6 -5 -4.5 -3 -2 -1 0 1 1 1 0 0 -0.5 -0.5 0 0
-0.5 -0.5 -0.5 -2 -2.5 -3.5 -4 -4.5 -6];
G(4,:) = [-8 -7 -4.5 -4 -3 -2.5 -2 -1 -1 -1 -1 -1 -1 -1
-1 -1 -1 -1 -2 -2 -3 -4 -4.5 -6 -7];
G(5,:) = [-9 -8 -6.5 -6 -4 -4 -3 -3 -2 -2 -2.5 -2 -2 -2
-2 -2 -2 -2.5 -3 -3.5 -4 -5 -6 -7 -8];
Gain = mean(G);
x = 10*log10(cos(angle/180*pi));
f1 = fit(x',Gain','poly1')
```

```
figure(1)
plot(f1,x,Gain)
xlabel('10*log(cos(\alpha))')
ylabel('Gain: dB')
title('Curve')
% linear fit based on firefly algorithm
clear;clc;close all
instr=[100 2000];
div=2;% p0,alpha
n=instr(1);
G=instr(2);
rand('state',0);
range=[0 200];
xrange=range(2)-range(1);
alpha=0.02;
gamma=1.0;
[xn,Lightn]=init_ffa(n,range,div);
maxo=zeros(1,G);
for t=1:G
    [zn]=f(xn,div,n);
    [Lightn,Index]=sort(zn);
    xo=xn;
    zo=zn;
    maxo(t)=Lightn(1);
    u=Index(1);
    if u==n
        m=u-1;
    else
        m=u+1;
    end

[xn]=ffa_move(xn,Lightn,xo,zo,alpha,gamma,range,t,n,xra
nge,div);
end
bb = Index(1)
xn(:,bb)
semilogy(maxo,'r:.')
best = maxo(1,G)

function [zn]=f(xn,div,n)
```

```
zn=zeros(1,n);
d = [0.65 0.87 1.13 1.40 1.61 1.87 2.27];
d_log = 10*log10(d);

p0=[38.2090, 30.7970, 26.8820, 30.5330, 27.6570,
27.6580, 29.6480]';
p30=[35.0415, 28.5745, 27.7675, 24.4230, 29.3350,
26.7490, 25.1185]';
p60=[27.2120, 27.2160, 23.4780, 24.6110, 23.6260,
23.1405, 22.3555]';
for j=1:n

    zn(1,j)=zn(1,j)+sum((p0-
xn(2,j)+xn(1,j)*log10(d)).^2)+...
        sum((p30-xn(2,j)+xn(1,j)*log10(d)-
22*log10(cos(30/180*pi))).^2)...
        +sum((p60-xn(2,j)+xn(1,j)*log10(d)-
22*log10(cos(60/180*pi))).^2);

end

end
function [min]=fb(xn)
div=1;
min=0;
for i=1:div
    min=(i*xn(i,1)^2)+min;
end
end
function [xn,Lightn]=init_ffa(n,range,div)
xrange=range(2)-range(1);
xn=rand(div,n)*xrange+range(1);
Lightn=zeros(1,n);
end
function
[xn]=ffa_move(xn,Lightn,xo,zo,alpha,gamma,range,t,n,xra
nge,div)
for i=1:n
    for j=1:n
        R=0;
```

```
        for l=1:div
            R=(xn(l,i)-xn(l,j))^2+R;
        end
        r=sqrt(R);
        if zo(i)>zo(j)
            beta0=1.0;
            beta=beta0*exp(-gamma*(r^2));
            for l=1:div
                xn(l,i)=xn(l,i) +beta*(xn(l,j)-
xn(l,i))+alpha*(rand-0.5)*xrange;
                if xn(l,i)>range(2)
                    xn(l,i)=range(2);
                elseif xn(l,i)<range(1)
                    xn(l,i)=range(1);
                end

            end
        end
    end
end
end
% antenna pattern curve fit
clear; clc; close all
angle = [-60:5:60];
G(1,:) = [-5.5 -4 -3 -2 -1.5 0 0 1 1.5 2 2 1 0 0 0 0 0
0 0 -1 -2 -3 -4 -4 -6];
G(2,:) = [-5.5 -4.5 -3.5 -2.5 -1.5 -0.5 0 1 1 1 0 0 0 0
0 0 0 0 0 -1.5 -2 -3 -4 -4 -6];
G(3,:) = [-6 -5 -4.5 -3 -2 -1 0 1 1 1 0 0 -0.5 -0.5 0 0
-0.5 -0.5 -0.5 -2 -2.5 -3.5 -4 -4.5 -6];
G(4,:) = [-8 -7 -4.5 -4 -3 -2.5 -2 -1 -1 -1 -1 -1 -1 -1
-1 -1 -1 -1 -2 -2 -3 -4 -4.5 -6 -7];
G(5,:) = [-9 -8 -6.5 -6 -4 -4 -3 -3 -2 -2 -2.5 -2 -2 -2
-2 -2 -2 -2.5 -3 -3.5 -4 -5 -6 -7 -8];
Gain = mean(G);
x = 10*log10(cos(angle/180*pi));
f1 = fit(x',Gain','poly1')
figure(1)
plot(f1,x,Gain)
xlabel('10*log(cos(\alpha))')
```

```
ylabel('Gain: dB')
title('Curve')

% PS model in corridor
clear;clc;close all
d = [0.78 0.87 1.04 1.13 1.31 1.53 1.65 1.70 1.83
2.04];
d_log = 10*log10(d);
p = [103.10 102.66 100.56 99.43 97.08 97.33 98.31 99.68
99.18 98.62];
f1 = fit(d_log',p','poly1')
plot(f1,d_log,p)
xlabel('10*log10(d)')
ylabel('Relative Power: dB')
title('Corridor Scenario')

disp('when alpha is 1.068')
disp('Mean value of shadow fading is:');
disp(mean(p-100.9+1.068*d_log));
disp('Standard Deviation of shadow fading is:');
disp(std(p-100.9+1.068*d_log));
figure(2)
scatter(d,p)
y = -10.68*log10(d) + 100.9;
hold on
plot(d,y)
hold off
xlabel('Distance of the object (m)')
ylabel('Relative Power (dB)')
```

% Distance between TX and RX is 7.5 meters

% RSSI RX: -51 dB TX: -55 dB

% pi model in corridor

clear;clc;close all

% -60, -30, 0, 30, 60 degrees

r = [0.65 0.87 1.13 1.40 1.61 1.87 2.27];

r_log = 10*log10(r);

```
% distance at 0.65 meters
p1(:,1) = [56.66 66.38 62.34 69.14 72.21 62.33 58.64 66.67 65.54 66.67]';
p1(:,2) = [75.16 72.62 75.94 73.88 79.14 72.21 75.73 68.17 72.81 74.19]';
p1(:,3) = [76.14 83.91 74.76 78.11 73.85 81.65 82.85 77.11 76.10 77.61]';
p1(:,4) = [76.38 76.13 74.91 71.62 70.52 76.16 77.89 80.27 79.24 77.86]';
p1(:,5) = [70.17 68.76 77.17 63.27 68.14 75.22 66.95 70.11 67.07 70.80]';
p_avg(1,:) = mean(p1)-40;
% distance at 0.87 meters
p2(:,1) = [68.83 67.92 63.40 69.52 72.43 69.74 66.73 64.97 63.94 64.88]';
p2(:,2) = [70.67 73.94 69.04 66.70 71.24 62.21 65.91 65.29 67.42 63.67]';
p2(:,3) = [71.21 63.59 73.72 70.33 73.91 75.63 73.88 69.83 66.51 69.36]';
p2(:,4) = [76.36 68.64 64.78 67.95 74.03 68.42 61.74 64.72 75.76 73.00]';
p2(:,5) = [69.08 70.49 69.46 61.40 71.43 67.48 67.89 65.22 71.25 58.26]';
p_avg(2,:) = mean(p2)-40;
% distance at 1.13 meters
p3(:,1) = [57.95 60.65 61.12 63.22 62.22 62.27 64.94 60.11 65.13 63.03]';
p3(:,2) = [63.15 67.98 72.09 68.52 69.33 66.00 62.49 71.36 72.84 65.37]';
p3(:,3) = [69.68 70.84 62.46 64.88 68.95 63.03 64.19 69.71 65.69 69.39]';
p3(:,4) = [64.75 72.68 70.62 71.71 70.52 62.21 68.36 65.59 66.69 63.09]';
p3(:,5) = [70.17 62.43 63.87 62.02 66.95 65.88 63.75 66.67 58.83 68.35]';
p_avg(3,:) = mean(p3)-40;
% distance at 1.40 meters
p4(:,1) = [62.09 67.23 62.43 64.78 66.76 62.81 62.34 60.74 57.67 61.18]';
p4(:,2) = [59.08 58.70 65.81 65.37 60.80 59.89 64.69 63.84 66.22 68.58]';
p4(:,3) = [70.77 71.93 74.94 72.28 73.81 69.24 70.93 64.53 67.04 69.86]';
```

```
p4(:,4) = [66.66 68.64 61.15 58.48 64.22 61.96 71.68 64.03 73.06 65.60]';
p4(:,5) = [67.54 67.48 58.07 61.46 66.98 69.08 68.67 72.09 71.33 61.49]';
p_avg(4,:) = mean(p4)-40;
% distance at 1.61 meters
p5(:,1) = [62.87 60.77 58.51 63.59 59.39 64.87 63.87 62.36 62.18 65.57]';
p5(:,2) = [62.80 69.51 64.97 69.99 65.09 61.36 73.56 71.96 67.83 69.42]';
p5(:,3) = [67.95 67.10 71.08 68.17 70.83 64.03 67.29 64.69 66.85 68.58]';
p5(:,4) = [68.42 71.46 72.78 76.07 70.89 73.28 66.69 70.77 72.81 67.04]';
p5(:,5) = [69.43 66.92 64.59 64.82 51.36 66.41 64.53 67.38 66.38 66.72]';
p_avg(5,:) = mean(p5)-40;
% distance at 1.87 meters
p6(:,1) = [69.11 64.41 60.29 59.42 66.79 59.86 62.53 64.91 60.61 62.84]';
p6(:,2) = [61.74 61.89 66.35 64.41 68.86 63.75 64.94 69.99 63.78 69.17]';
p6(:,3) = [68.20 67.14 68.95 62.43 68.08 68.42 72.75 67.04 68.92 64.65]';
p6(:,4) = [69.64 67.26 62.87 66.10 68.51 66.63 69.64 68.92 70.64 69.89]';
p6(:,5) = [63.81 63.37 59.80 68.89 67.20 62.68 58.38 67.76 58.41 61.74]';
p_avg(6,:) = mean(p6)-40;
% distance at 2.27 meters
p7(:,1) = [61.49 67.44 56.07 58.36 64.59 63.40 62.62 56.73 62.55 59.83]';
p7(:,2) = [65.63 62.50 65.44 66.41 66.29 65.66 67.51 68.04 60.83 67.57]';
p7(:,3) = [68.79 68.33 69.05 67.48 67.70 76.22 71.87 72.05 69.58 65.41]';
p7(:,4) = [66.38 61.02 64.03 59.67 70.14 65.37 64.18 68.92 63.91 62.87]';
p7(:,5) = [69.27 58.20 61.27 68.67 60.55 65.47 63.16 65.19 63.87 58.38]';
p_avg(7,:) = mean(p7)-40;
% data processing
```

```
p60 = 0.5*(p_avg(:,1)+p_avg(:,5));
p30 = 0.5*(p_avg(:,2)+p_avg(:,4));
p0 = p_avg(:,3);
% % liner fit
figure(1)
f1 = fit(r_log', p0, 'poly1')% -1.41 31.78
plot(f1, r_log, p0')
hold on
f2 = fit(r_log', p30, 'poly1')% -1.418 29.74
plot(f2, r_log, p30')
f3 = fit(r_log', p60, 'poly1') % -0.6214 22.25
plot(f3, r_log, p60')
hold off


% p0 32.44
% p30 30.39
% p60 23.80
figure(2)
hold on
scatter(r_log,p0','r')
scatter(r_log,p30','g')
scatter(r_log,p60','b')
y0 = -2*r_log+32.44;
y30 = -2*r_log+30.39;
```

```
y60 = -2*r_log+26.77;
plot(r_log,y0,'r')
plot(r_log,y30,'g')
plot(r_log,y60,'b')
legend('incident angle=0\circ','incident angle=30\circ',...
   'incident angle=60\circ')
xlabel('10*log10(d)')
ylabel('Relative Power: dB')
title('CWINS Laboratory Scenario')
% mean and std
disp('For the degree is 0')
disp('Mean value of shadow fading is:');
disp(mean(p0'-32.44+2.0*r_log));
disp('Standard Deviation of shadow fading is:');
disp(std(p0'-32.44+2.0*r_log));

disp('For the degree is 30')
disp('Mean value of shadow fading is:');
disp(mean(p30'-30.39+2.0*r_log));
disp('Standard Deviation of shadow fading is:');
disp(std(p30'-30.39+2.0*r_log));

disp('For the degree is 60')
disp('Mean value of shadow fading is:');
disp(mean(p60'-26.77+2.0*r_log));
```

```
disp('Standard Deviation of shadow fading is:');
disp(std(p60'-26.77+2.0*r_log));
%-20*log10(d)+17.8913*log10(cos(a))+32.0121

%-12.9400*log10(d)+18.2056*log10(cos(a))+31.2233

figure(3)
% set a as 2
hold on
scatter(r_log,p0','r')
scatter(r_log,p30','g')
scatter(r_log,p60','b')
y0 = -20*log10(r)+17.8913*log10(cos(0))+32.0121;
y30 = -20*log10(r)+17.8913*log10(cos(30/180*pi))+32.0121;
y60 = -20*log10(r)+17.8913*log10(cos(60/180*pi))+32.0121;
%%%%%%%
aaa = [(p0'-y0) (p30'-y30) (p60'-y60)];
%%%%%%%
plot(r_log,y0,'r')
plot(r_log,y30,'g')
plot(r_log,y60,'b')
legend('incident angle=0\circ','incident angle=30\circ',...
    'incident angle=60\circ')
xlabel('10*log10(d)')
ylabel('Relative Power: dB')
```

```
title('Corridor Scenario (\alpha=2)')
hold off

disp('When set alpha as 2:')
disp('Mean value of shadow fading is:');
disp(mean(aaa));
disp('Standard Deviation of shadow fading is:');
disp(std(aaa));




figure(4)
hold on
scatter(r_log,p0','r')
scatter(r_log,p30','g')
scatter(r_log,p60','b')
y0 = -12.9400*log10(r)+18.2056*log10(cos(0))+31.2233;
y30 = -12.9400*log10(r)+18.2056*log10(cos(30/180*pi))+31.2233;
y60 = -12.9400*log10(r)+18.2056*log10(cos(60/180*pi))+31.2233;
bbb = [(p0'-y0) (p30'-y30) (p60'-y60)];
plot(r_log,y0,'r')
```

```
plot(r_log,y30,'g')
plot(r_log,y60,'b')
legend('incident angle=0\circ','incident angle=30\circ',...
    'incident angle=60\circ')
xlabel('10*log10(d)')
ylabel('Relative Power: dB')
title('Corridor Scenario (linear regression)')

disp('When linear regression:')
disp('Mean value of shadow fading is:');
disp(mean(bbb));
disp('Standard Deviation of shadow fading is:');
disp(std(bbb));
hold off
p0 = p0+40;
p30 = p30+40;
p60 = p60+40;
figure(5)
hold on
scatter(r,p0','r')
scatter(r,p30','g')
scatter(r,p60','b')
y0 = -12.56*log10(r)+22*log10(cos(0/180*pi))+71.68;
y30 = -12.56*log10(r)+22*log10(cos(30/180*pi))+71.68;
y60 = -12.56*log10(r)+22*log10(cos(60/180*pi))+71.68;
```

```
plot(r,y0,'r')
plot(r,y30,'g')
plot(r,y60,'b')
legend('\alpha=0\circ','\alpha=30\circ',...
   '\alpha=60\circ')
xlabel('Distance of the interference source (m)')
ylabel('Relative Power (dB)')
hold off
dme = [p0'-y0 p30'-y30 p60'-y60]';
mean(dme)
std(dme)
```